International Journal of Biological Macromolecules 143 (2020) 1009–1032

Contents lists available at ScienceDirect

International Journal of Biological Macromolecules

journal homepage: www.elsevier.com/locate/ijbiomac

Anti-inflammatory effect of epidermal growth factor conjugated silk fibroin immobilized polyurethane ameliorates diabetic burn wound healing

Sohini Sen [a,1], Piyali Basak [a,1], Bishnu Prasad Sinha [b], Praveen Maurye [c], Krishna Kumar Jaiswal [d], Partha Das [e], Tapan Kumar Mandal [b,*]

[a] School of Bioscience & Engineering, Jadavpur University, India
[b] Veterinary Pharmacology & Toxicology, West Bengal University of Animal & Fishery Science, India
[c] Fishery Resource and Environmental Management Division, Central Inland Fisheries Research Institute, India
[d] Centre for Green Energy Technology, Pondicherry University, India
[e] Veterinary Anatomy, West Bengal University of Animal & Fishery Science, India

ARTICLE INFO

Article history:
Received 22 May 2019
Received in revised form 22 September 2019
Accepted 23 September 2019
Available online 21 October 2019

ABSTRACT

Few studies are reported on immunomodulatory potential of non-mulberry (*Antheraea mylitta*) silk fibroin (SF) combined with polyurethane (PU) in diabetic wound healing. In this study, PU/SF (*Antheraea mylitta)* scaffolds were fabricated by blending and immobilization techniques. Effective SF dosage was determined and incorporated according to minimum inhibitory concentrations against wound associated bacterial strains while fabricating scaffold. Dermal fibroblast NIH3T3 cells were seeded on epidermal growth factor (EGF) treated and untreated PU/SF scaffolds, fabricated by blending and immobilization techniques. Fibroblast seeded PU/SF scaffolds were investigated for anti-inflammatory response in wound recovering potential comparing with Acticoat™ in third degree burn of streptozotocin induced diabetic rats. At 16th, 24th days, promising healing was achieved with faster granulation, enhanced collagenization, patterned re-epithelialization by EGF treated cellular immobilized PU/SF in normal, hyperglycemic burn. Biomarkers of different healing stages, CD31 (haemostasis), Ki67 (proliferative), alpha-sma, COL III (maturation) were examined. Since hyperglycemic burn is characterized by inflated pro-inflammatory cytokines, serum, tissue IL-6,8,10 were recorded, which revealed timely restoration of inflated IL-6,8 and protection against IL-10 elevation by cellular immobilized PU/SF compared to Acticoat™ ($p \leq 0.05$), control ($p \leq 0.01$). E-cadherin (gap junction protein), MMP 9 response suggested anti-inflammatory role of PU/SF on accelerated healing of thermal injury as potent dermal substitute.

1. Introduction

Impaired wound healing is concomitant with diabetes with complex patho- physiological phenomenon and the prolonged inflammation along with increased oxidative stress impairs healing process in diabetes. In 2015, 170 million deaths were caused due to diabetes, among which 20.8 million was in USA [1], and this data are projected to be double by 2030 [2]. Around 25% diabetic populations shall suffer from diabetic foot ulcers in coming decades, which will necessitate efficient diabetic wound management speculated by World Health Organization (WHO) [3,4]. Non-fatal chronic burn injury is a global public health crisis leading to morbidity. Acute thermal injuries requiring medical treatment affect nearly half a million Americans each year, with approximately 40,000 hospitalizations and 3400 deaths annually [5]. People of lower middle socioeconomic countries are at higher risk like sixty seven percent burn cases are witnessed in Africa and South-East Asia reg-ions [6]. Therefore, diabetic burn wound management is a craving issue which should include blood sugar control, removal of wound exudate and dead tissue, early resuscitation, wound excision and coverage, infection management and proper choice of wound dressings is required in the fight against burn mortality. Topical dressings research for third degree full thickness burn is overall poor as each category of dressings has individual merits and demerits. Non-adhesive dressings are inexpensive, well tolerated; foam and alginate dressings are absorbent thus effective for heavily exuding wounds. Dressings containing inidine and silver aid in managing wound infection whereas occlusive dressings

* Corresponding author.
E-mail address: drtkm48@gmail.com (T. Kumar Mandal).
[1] Both the authors contributed equally.

https://doi.org/10.1016/j.ijbiomac.2019.09.219
0141-8130/

should be avoided for infected wounds. Most of dressings require frequent change to reduce maceration for faster healing. Unfortunately, none of these stimulate all the four phases of healing process for burn wound repair. Dressing choice should be guided by wound characteristics, exact requirements and cost effectiveness. Grafting is popular alternative to third degree burn patients, but failure due to graft rejection is still challenging to effective diabetic burn wound healing. Thus, popularity of tissue engineered graft is gaining importance gradually. Trends in such wound treatments are exploiting disinfectants including application of epidermal growth factor (EGF)-containing formulations around lesions area [7,8]. Therefore, this study explored the potential of EGF incorporated tissue engineered scaffold. Specific regulatory markers play pivotal role in upregulation or downregulation of healing response in each phase.

Polyurethane (PU) has already been used as wound healing agent in commercial dressings like Tegaderm™, Bioclusive™ [9–11] due to high biocompatibility, appreciable swelling ability, cell adhesive nature, nonimmunogenic and appreciable mechanical strength. Additionally, non-mulberry silk fibroin (SF) is reported as efficient wound healing agent as they have antimicrobial property and offer enriched Arginine, Glycine and Aspartate (RGD sequences), facilitating binding to integrin receptors of cell membrane, which provides functional advantage of mediating cell-material interactions for wound repair being responsible for extracellular matrix components (ECM) synthesis [12]. Earlier studies showed mulberry (Bombyx mori) silk fibroin coated polyurethane matrix has greater affinity to fibroblast cell adhesion and proliferation [13], and it did not elicit any assayable amount of three main proinflammatory cytokines, namely interleukin-1β (IL-1β), tumor necrosis factor-alpha (TNF-α), and transforming growth factor-β1 (TGF-β1) when human fibroblasts cultured on PU scaffolds [14]. Independent studies reveal antimicrobial potential of mulberry *Bombyx mori* and non-mulberry *Antheraea mylitta* silk fibroin [15] and *Antheraea mylitta* variety SF are richer in RGD sequences compared to Bombyx mori variety [16] and customized PU scaffold architecture helped to release SF from matrix. *Antheraea mylitta* SF was chosen in optimum dose of effective inhibitory concentration to combat with microbial invasion that could be beneficial for eliminating burn associated infection and a novel effective route of surface immobilization of SF onto PU microporous scaffold has been proposed. As in diabetic patients, wound healing process is delayed; this study aims to investigate diabetic burn wound healing efficiency of PU/SF hybrid mats, applied topically on streptozotocin induced diabetic wistar rats a long with its immunomodulatory effects followed by biochemical parameters. Synergistic effect of PU and SF protein (*Antheraea mylitta*), is not reported on hyperglycemic burn wound healing and no study is available on prospective immune-modulatory role of PU/SF (*Antheraea mylitta*), or biological insight on alteration in inflammatory response [17] by topical application of PU/SF on diabetic burn have not been investigated so far. In our earlier studies, exploiting standard strategies of blending, Isophorone diisocyanate (IPDI) based PU was employed for scaffold fabrication with precise pore size suitable for fibroblast and keratinocytes proliferation and dose determined SF (*Antheraea mylitta*), was immobilized on surface functionalized porous PU scaffold for topical application.

Wound healing involves complex mechanism with independent stages of hemostasis, inflammatory, proliferative and maturation - remodelling phases. Relative delay in chronic hyperglycemic wound is attributed by lack of periodic activation of cascading molecules due to inflammation which triggers sequential recruitment of inflammatory cells, neovascularization and re-epithelialization [18]. Specific regulatory markers play pivotal role in upregulation or downregulation of healing response in each phase. Relative response of representative signature markers from each healing phase i.e. angiogenesis promoting CD31, proinflammatory cytokines like IL-6, IL-8 and IL-10 response in inflammatory phase, keratinocytic migration indicative Ki67 accumulation in proliferative phase [19], alpha sma, COL III expression in maturation phase was investigated. In context of wound re-epithelialization, cell adhesion and gap junction mediating cell surface protein E-cadherin is of prime importance for retaining cytoskeletal integrity of epithelium and controlling cellular polarity, differentiation, growth, and migration of cells [20]. Thus expression pattern of E-cadherin was also studied in both hyperglycemic and non-hyperglycemic wound. PU/SF scaffolds have shown appreciable antimicrobial efficiency as evidenced by treating with E. coli, S. aureus, P. aeruginosa and K. pneumonia etc. Moreover, it is advantageous as occasional requirement of dressing change is attributed by its high absorbent nature whereas, Acticoat™ required a mandatory dressing replacement at 3 days interval in wet condition. This study provides convincing experimental evidence that immobilized non-mulberry SF (*Antheraea mylitta*) with PU mutually served as an attenuating factor of burn associated proinflammatory cytokines contributing to hyperglycemic burn wound healing process which suggests this may be used to treat burn patients with diabetes.

2. Experimental

2.1. Silk fibroin (SF) isolation

Non-mulberry silkworm *(A. mylitta)* silk fibroin was isolated following the earlier described protocol [21]. Well grown non-mulberry silkworm *(A. mylitta)* larvae fifth instar stage was procured and silk glands were thoroughly washed with de-ionized water to remove debris. First silk glands were dissected, and fibroin protein was squeezed out from the glands manually. SF protein was dissolved in aqueous solution of 1% w/v sodium dodecyl sulfate (SDS) buffer, 5 mM EDTA, and 10 mM Tris (pH 8.0) in stirring condition. SDS was utmost removed by dialyzing SF solution using cellulose membrane-based dialysis cassette (MW 12.4 KDa) extensively upto 48 h against Milli Q water at 4 °C. Dialyzed SF within dialysis membrane (MW 3.5 KDa) was concentrated in polyethylene glycol at room temperature for 1 h. Reconstituted SF was stored at 4 °C.

2.2. Determination of minimal inhibitory concentration (MIC) of SF for dose selection

The minimum inhibitory concentration (MIC) was determined following the method described by Bhowmick et al [22] against *Escherechia coli* (ATCC 25922), *Staphylococcus aureus* (ATCC 6538), *Pseudomonus. aeruginosa* (ATCC 15442), *Klebsiella pneumoniae* (ATCC *6538)* obtained from microbial repository of MTCC, IMTECH, Chandigarh, India. In brief, all the strains were cultured on Leuria broth at 37 °C for 24 h, and appropriate dilutions were made from the fresh liquid cultures to get final bacterial cell concentration of 10^8 CFU/ml to begin with MIC experiment respectively. Bacterial cell count was based on the absorbance value of 0.1 OD at 600 corresponding to 10^8 cells/ml. The concentration of SF chosen for all the four strains were adjusted from 4 mg/ml to 8 mg/ml. The lower cut off 4 mg/ml was preselected based on random dose selection ranging from 200 μg/ml to 4 mg/ml. For first screening, ranging from 200 μg/ml to 3.8 mg/ml, 250 μl of adjusted bacterial solution (CFU ~ 10^8) along with 250 μl of different concentration of SF (200 μg/ml to 4 mg/ml) were added to 48 well plate and incubated at 37° C upto 72 h. During this entire period, optical density at 600 nm was recorded at various time points to obtain the growth curve and rapid growth was found below the doses of 3.8 mg/ml. Therefore, second screening range was considered from 4 mg/ml

to 8 mg/ml following the same procedure described as above and final determined minimal inhibitory SF concentration was considered for incorporating into all the different variety of scaffolds.

2.3. Preparation of PU/SF microporous matrices by blending and immobilization employing surface aminolysis technique

Isophorone diisocyanate (IPDI, TCI, MW. 222.29) was dissolved in Dimethyl sulphoxide (20 ml) and Polyethylene glycol (PEG, MERK, MW. 400) was added with continuous stirring for 45 min at 120 °C. The molar ratio of IPDI and PEG 400, i.e. (diisocyanate, NCO: polyol, OH) was taken as 2:1 to ensure complete reaction between free NCO and OH groups. Dibutylitin dilaurate (DBTDL, Sigma Aldrich) was added dropwise as catalyst followed by addition of 2-propanol to reaction mixture [23]. This reaction could take place for 1 h to block the free isocyanate groups. Regenerated SF solution (8 ml) was mixed into it and Genipin (Sigma Aldrich, 1 ml) was used as a cross-linker to facilitate the polymer synthesis. After silk protein was completely dissolved, a blended viscous yellowish solution was obtained. Therefore, polymer was crystallized at −80° C for 27 h and followed by lyophilizing at −80° C for 48 h. The matrix obtained was vaccum dried under room temperature and stored in desiccator for further use.

Likewise, IPDI based scaffold was fabricated as described without SF by lyophilization. The lyophilized matrix was vaccum dried under room temperature and subjected to surface modification [24]. Scaffolds were immersed in 7 wt% 1,6-hexane diamine solution (60 mg/ml) in 2-propanol for 10 to 15 min at 37 °C to aminolyze the matrix followed by extensive washing with distilled water for 24 h to remove free unbound 1,6-hexane diamine from scaffold surface. Then the membrane was dried overnight, incubated in Glutaraldehyde solution (1.5% (w/v)) for 3 h at room temperature to convert surface exposed amino groups into aldehyde groups. This was followed by extensive rinsing with large amount of deionized water to make the surface Glutaraldehyde free. SF (8 mg/ml as calculated highest MIC value) was immobilized on PU scaffold surface by incubating the modified PU scaffolds in SF protein for 48 h at 4 °C (Fig. 2f). Scaffolds were washed with PBS thrice to remove unbound or loosely bound SF and debris, which ensured the presence of only immobilized SF on the scaffold surface.

2.4. Characterization of PU/SF scaffold

Scanning electron microscopy was performed to investigate surface morphology of the scaffolds and to confirm the presence of interconnected pores. Interconnected pores facilitate the fibroblast cells to proliferate well in scaffold architecture. Scaffolds were fractured in liquid nitrogen for cross-sectional analysis followed by platinum coating and images were captured with a JEOL MAKE (UK) MODEL-JSM 6360 scanning electron microscope at an accelerating voltage of 20 KV.

Atomic force microscopic (AFM) studies evaluated the surface roughness and microstructure of the scaffold varieties including their three-dimensional structures. Herein, vacuum dried PU/SF scaffolds were placed on the holder with the aid of carbon coated tape and scanned under tapping mode using AFM (Multiview 3000, Nanonix Imaging Limited, Israel).

Water uptake study was performed to evaluate the phosphate buffer saline (PBS, pH 7.4) retaining capacity of the scaffold matrix [25]. The scaffolds were tailored into square shape of 4 cm^2 area and dry weight were measured. Dried and pre-weighed scaffolds were immersed in PBS and water. After specific intervals, swollen scaffolds were taken out of water and PBS and wet weight were recorded after wiping surface gently over blotting paper. This study was performed upto 24 h and degree of water uptake was calculated as per the following equation:

$$\text{Percent water uptake} = \frac{\text{maximum wet weight} - \text{initial dried weight}}{\text{initial dried weight}} \times 100(\%) \quad (1)$$

2.5. Recombinant rat specific epidermal growth factor (rEGF) loading into PU/SF matrix and mathematical modelling of SF and rEGF release profile

Rat specific recombinant epidermal growth factor (SRP3238, Sigma Aldrich, recombinant, expressed in *E. coli*, ≥98% (SDS-PAGE), ≥98% (HPLC) vial was centrifuged before reconstitution. Reconstitution was done to 100 μg/ml concentration in millipore water containing 0.1% bovine serum albumin (BSA, 100 μg/ml). Reconstituted rat rEGF was incorporated into scaffolds at 20 μg/ml concentration.

Herein the scaffolds were immersed into PBS at 37 °C and cumulative percent SF release at different time intervals were calculated [26] and then it was compared with different kinetic models.

Rat specific rEGF incorporated scaffolds were immersed into PBS and allowed to elute rEGF. Cumulative SF and rEGF release profile were calculated by Equation no 3, where M_t is the amount of rEGF released at time t and M is the theoretical value of rEGF, loaded in scaffold. The release kinetics of SF and rEGF from immobilized and blended PU/SF in PBS were studied by release kinetic theories like Higuchi kinetics, Korsmeyer-Peppas kinetic models using Eqs. (3) and (4) respectively, where M_t/M is the fraction of release in time t and M_t is amount of release at time t, n is diffusion exponent which recognizes its fickian or non-fickian nature of release pattern; $n \leq 0.5$ indicates fickian and $0.5 < n \leq 1$ represents non-fickian mechanism.

$$\text{Percent SF or rEGF release} = \frac{Mt}{M} \times 100 \quad (2)$$

$$\frac{Mt}{M} = K \times tn \quad (3)$$

$$Mt = k \times \sqrt{t} \quad (4)$$

2.6. In vitro NIH3T3 cell line maintenance on PU/SF scaffold

3 cm discs of EGF treated and untreated PU/SF scaffolds were sterilized at 1.5 lb/ $inch^2$ pressure, 121° C for 20 min. Mouse foreskin fibroblast (NIH3T3) cells growth to confluency was performed in a controlled atmosphere (Leishmen Sanghai CO_2 Incubator 37° C, 5% CO_2) using Dulbecco's Modified Eagle's Medium (DMEM, Hi-Media, India), supplemented with 10% Fetal Bovine Serum (FBS, Hi-Media, India) and Penicillin-streptomycin antibiotic solution (Hi-Media, India). Confluent monolayers were propagated by trypsinization (0.25% Trypsin and 0.02% EDTA, Hi- Media, India) and re-plated at 72 h. EGF treated and untreated PU/SF scaffolds were pre-incubated in complete media in the six well microtitre plate overnight. At third passage of cell maintenance, cells were seeded on the preincubated EGF treated and untreated PU/SF scaffolds at seeding density of 2×10^5 cells/well followed by incubation upto 24 h. These NIH3T3 cell seeded, EGF treated and untreated PU/SF scaffolds were applied at the burn wound site.

2.7. In vivo wound healing

2.7.1. Diabetic burn wound model development

The animal protocol was performed following approval of Institutional animal ethics committee (vide letter no: AEC/PHARM/1702/22/2017). A standard full thickness burn wound

model was established for evaluating efficiency of blended and immobilized varieties scaffolds compared to commercial treatment Acticoat™ (Smith & Nephew, Inc.) as wound dressing in rat model (*Rattus norvegicus*). The experimental animals were divided into two groups i.e. diabetic and non-diabetic. Acticoat™ was replaced at every three days in wet condition as per manufacturer's instruction whereas PU/SF scaffolds treatments were changed at 10–11 days interval in dry condition. For induction of diabetes, Streptozotocin at 50 mg/kg body weight was intravenously injected to tail vein of the animals [27] and after 3 days of Streptozotocin (Table 4) administration, burn model was developed.

The rats were anesthetized by xylazine hydrochloride (12 mg kg^{-1} body weight) and ketamine hydrochloride (65 mg kg^{-1} body weight). A dedicated sterile red-hot metallic bar was held in contact with the shaved animal's dorsal skin for 12 s, following standard procedure for producing third-degree burn. Twenty percent dorsal body surface was burnt where surface was calculated by Meeh's formula $A = 10 \times W^{2/3}$, where: A = area in cm^2 and W = weight in grams. NIH3T3 cell seeded, EGF treated and untreated PU/SF scaffolds and Acticoat™ were applied at the burn wound. Animals were placed in aseptic and optimized lighting conditions (12 h light/dark photoperiod), at 25 °C. Wounded areas were washed thrice with seventy percent ethanol every day to maintain aseptic condition at the wound site. Wounded animals were euthanized at different interval to collect blood by direct heart puncture. Collected blood was centrifuged at 3000 rpm for 20 min and serum was separated and stored in liquid nitrogen. The healed tissue of wounded area was collected at those intervals for all the groups stored at −20 °C for biochemical estimations.

2.7.2. Wound healing index and tensile strength of regenerated skin

The burnt wound site in each group was photographed at different intervals (0th, 3rd, 7th, 14th, 21st days) for diabetic and normal wound. Lesion area was measured (mm^2) using Image J software (NIH, USA) and wound closure index was calculated following Eq. (5).

$$\text{Percent wound closure}(\%) = \frac{(\text{initial wound area at 0th day} - \text{wound area at nth day}) \times 100}{\text{initial wound area at 0th day}} \quad (5)$$

The healed skin was excised 3 weeks post burn from each group, ultimate tensile strength (UTS) and Young's Modulus of regenerated skin were evaluated in wet condition from initial breaking point in stress-strain curve obtained from Universal Testing Machine (UTM; Instron 4204, UK), under 100 N load cell. The wound strength was calculated as following Eq. (6):

$$\text{Wound strength}(\%) = \frac{\text{UTS of normal unwounded skin}}{\text{UTS of wounded skin}} \times 100 \quad (6)$$

2.7.3. Haemocompatibility and blood platelet adhesion study on PU/SF scaffold

In order to investigate the interaction between the blood cells and IPDI based PU/SF matrices, the haemolysis was analyzed by direct blood contact following earlier described method [28]. Briefly, anti-coagulated rat's blood was diluted with normal saline solution (8 ml blood and 10 ml N-saline) and N-saline (10 ml) was considered as positive control. The samples were incubated for 72 h at 37 °C in CMF-PBS (calcium and magnesium free Phosphate Buffered Saline). Fresh blood obtained by vein puncture in vacuum tubes containing sodium citrate (3.8%) in a ratio of 9:1 was used. Positive and negative controls were prepared by mixing 1 ml whole blood with 7 ml distilled water and CMF-PBS, 1 ml whole blood was kept as blank. The scaffolds were incubated for 3 h at 37 °C in the citrated blood, with slight agitation every 30 min. Afterwards, the scaffolds were removed, blood was centrifuged at 2000 rpm for 15 min, plasma separated, and following second centrifugation, the poor platelet plasma was isolated. After another centrifugation, supernatant was mixed with Drabkin reagent and the optical density was read at 546 nm. The hemolytic activity was calculated by direct contact method, according to ASTM F 756–00 standard. The formula used to calculate the hemolytic index is given in Eq. (7).

$$\text{Percent haemolysis} = \frac{[\text{OD test} - \text{OD negative control}] \times 100}{\text{OD positive control} - \text{OD negative control}]} \quad (7)$$

In order to investigate whether the blood platelets were susceptible to adhesion towards scaffold, resulting into platelet rupture or not, platelet adhesion study was performed following Chouhan et al. protocol [29].

2.7.4. Wound tissue hydroxyproline, hexosamine, elastin content estimation

In order to characterize regenerated full thickness skin, the deposited extra cellular matrix quantity had been estimated. The excised tissue was collected at different time intervals (day 7, 14 and 21) and stored at −80 °C to restore its ECM components. Tissues (100 mg) under −20 °C was thawed and chopped under ice cold condition [30]. Total tissue hydroxyproline, hexosamine and elastin content was estimated following the earlier described method [31–33].

2.7.5. Western blotting

All crude protein samples were analyzed on the protein slab gel (10%) using standard protocol (Laemmli 1979). Treated and control tissue were grinded with liquid nitrogen and lysed with precooled RIPA buffer (100 μl) and Protease inhibitor cocktail mix at 4 °C for 30 min followed by centrifugation at 13,000 rpm at 4 °C for 10 min. Supernatant was mixed with bromophenol blue, heated for 5 min at 95° C and subjected to SDS-PAGE with 10 percent running gel for 2 h [64]. Total protein was transferred to PVDF membrane using Amersham ECL semi dry blotting apparatus (GE Healthcare Life Sciences, USA) for 150 min followed by blocking with 5% BSA for 2 h and washed with TBST (Tris buffer saline with Tween 20) buffer. PVDF membrane was incubated with primary anti rat E-cadherin antibody (Elabscience, China) overnight at 4 °C followed by incubating it in secondary horseradish peroxidase conjugated IgG antibody (Elabscience, China) for 2 h. Then signals were detected following manufacturer's protocol using Excellent chemiluminescence kit (Elabscience, China).

2.7.6. Gelatin zymography

The expressions of MMP 9 in the tissue samples were studied by Gelatin Zymography. The 7 days treated, and control protein samples were loaded in individual wells of the protein slab gel (10%) and ran as per the standard protocol (Laemmli 1979) containing 15 mg/ml gelatin in resolving gel. After electrophoresis, gelatin zymography was performed following the protocol [34] to detect the presence of MMP 9 in all the tissue.

2.7.7. Pro-inflammatory cytokine analysis

Serum was collected, and wound tissue from all treatments including control groups were excised starting from 6 h to 14 days at different time points of postburn, homogenized in 10% PBS (pH 7.4) at 4° C. IL-6, IL-8, IL-10 levels, both of serum and tissue homogenate were quantified for the different intervals following manu-

facturer's protocol of rat specific IL-6, IL-10 ELISA kit (Elabscience, China) and IL-8 (Raybiotek, China).

2.7.8. Histomorphological analysis

Tissue sections were stained with H & E & Masson's trichome (MT) for histological examination of both kind of wounds over entire healing progression upto 21 days to justify the healing ability of all the four dressings varieties including Acticoat™ at different intervals. H & E and MT staining images were taken by considering 5 fields per specimen under bright field microscope (LEICA DM 2000) with image analysis software QWIN software Version 3.0. The healing information with different groups of treatment was scored on a scoring system based on few parameters [35] which are tabulated in Table 2.

2.7.9. Immunohistochemical staining

The tissue sections (8 μm) were subjected to immunostaining with anti-rat CD31 (Abcam, ab182981), anti-rat COL III (Abcam, ab6310), anti-rat Ki-67 (Abcam, ab16667), anti-rat alpha smooth muscle actin antibodies (Invitrogen, 1 A4 (asm-1). The sections were incubated with labeled secondary antibody, immunohistochemical study was performed following manufacturer's protocol of DAKO Envision Plus kit, for visualizing the antibody expression at different wound healing stages.

2.8. Statistical analysis

All the experiments were conducted in triplicate to get statistically significant result. All the data are expressed as mean ± standard deviation. Level of significance was evaluated at $^{*}p \leq 0.05$ to be significant, $^{**}p \leq 0.01$ to be moderately significant and $^{***}p \leq 0.001$ to be highly significant by one-way analysis of variance (ANOVA) using Tukey's post hoc test in Origin Pro. 9.0 analysis software.

3. Results

3.1. Minimal inhibitory concentration and dose selection of SF

Since antimicrobial property of mulberry SF already reported against a series of gram positive and gram-negative bacteria, this property was exploited to inhibit the microbial load at the wound bed. Though antimicrobial property of SF is known against *Escherichia coli*, *Staphylococcus aureus*, *Pseudomonus. aeruginosa*, *Klebsiella*

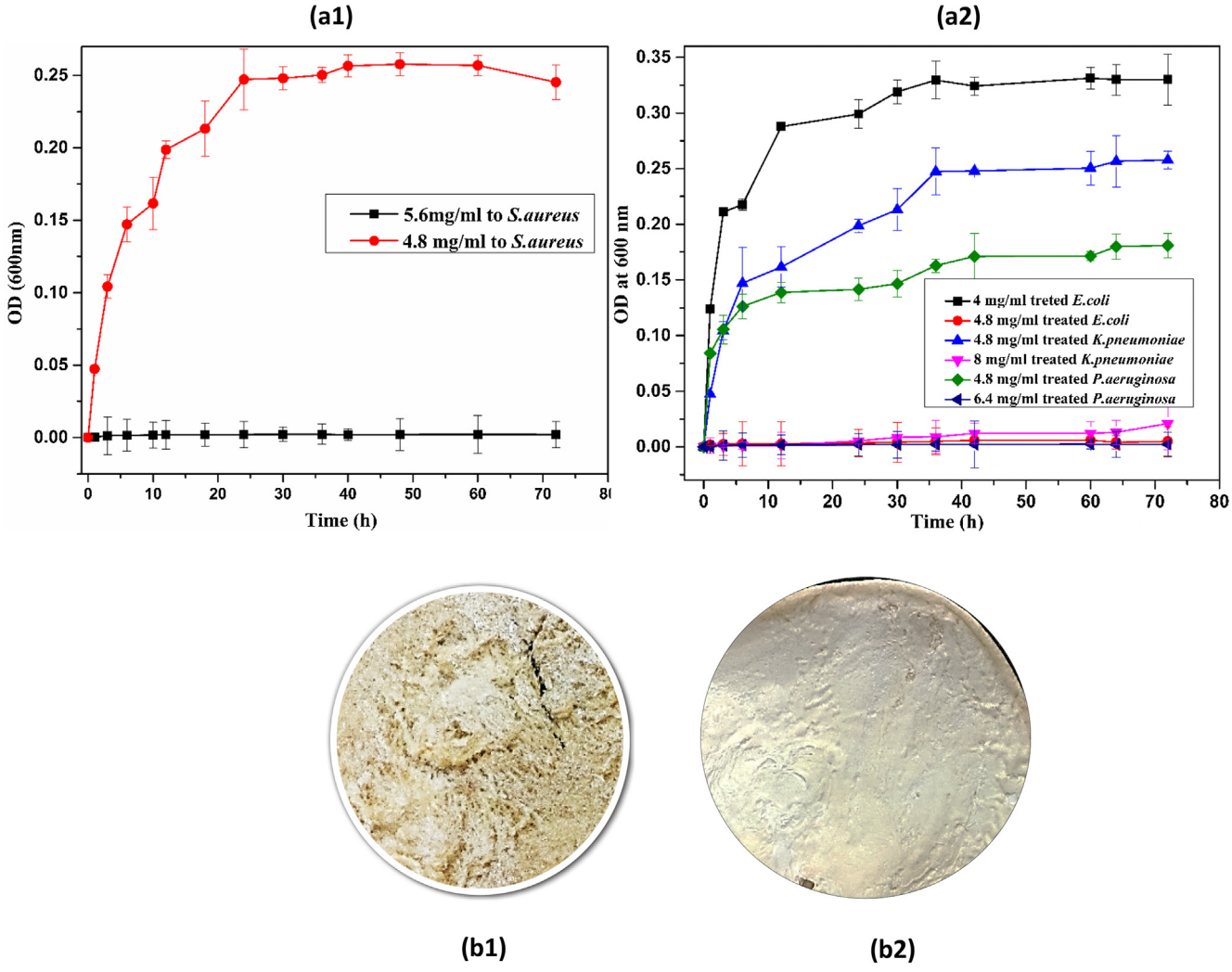

Fig. 1. a. Growth curve of a1. gram positive and a2. gram negative bacteria against various concentration of SF to determine minimal inhibitory concentration. Y-error bars represent standard deviation b. images of (b1) blended (b2) immobilized PU/SF scaffold c. Cumulative percent release of SF and rat specific rEGF in PBS, Release kinetics in d. Korsmeyer Peppas and e. Higuchi model of SF and rat specific rEGF from PU/SF blended and PU/SF immobilized scaffolds f. Schematic of scaffold fabrication process.

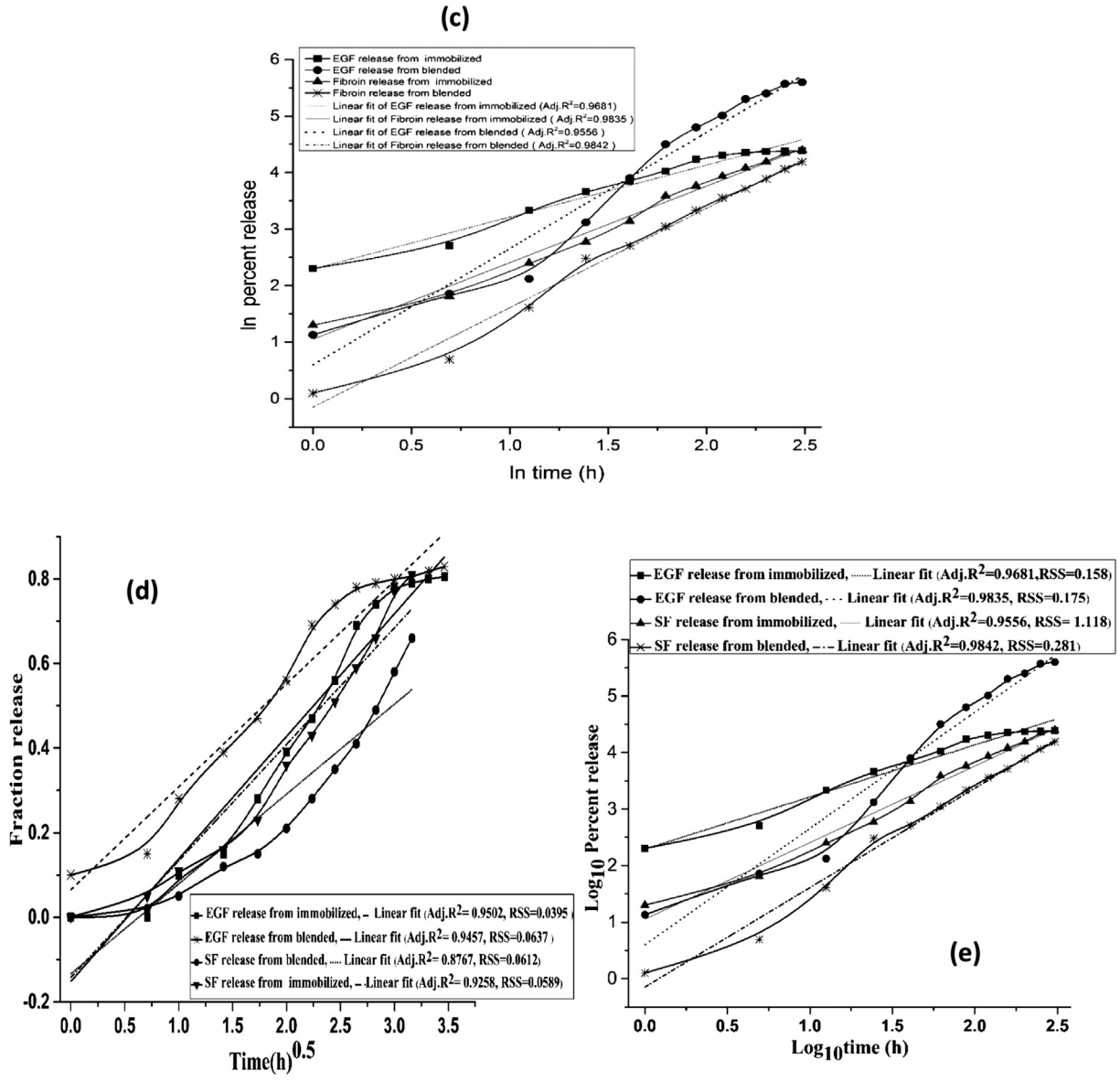

Fig. 1 (*continued*)

pneumoniae but its MIC has not been reported yet for these bacterial strains. In order to prevent bacterial infection at wound site, MIC of SF to these strains was determined to fix the desired concentration of SF to be incorporated into the scaffolds. Microbial load is often associated at the wound site, therefore wound dressing has an inherent antimicrobial potential not to adhere a wide range of microbes at the site, otherwise it will threaten the pace of healing progression [36]. Thus, it had been strategized that scaffolds must have antimicrobial activity not to exploit in vitro drug incorporation. Therefore, microbial resistivity of SF concentration was verified for individual strains. The antimicrobial property is attributed by synergistic effect of SF, and the hydrophobic interaction between PU and SF. Thus, at first 4 mg/ml SF concentration was chosen to investigate the microbial growth inhibitory effect to all four strains by measuring the OD_{600} values, but none was inhibited by this lower concentration. A little higher concentration was investigated for the purpose. Scaffold containing 4.8 mg/ml of SF was able to inhibit the *E. coli* population only whilst this concentration was inadequate to stop the growth of *S. aureus* and *P. aeruginosa*, *K. pneumoniae* as shown in Fig. 1(a.1) and Fig. 1(a.2) respectively. Then with random screening of the SF concentration it was found that 5.6 mg/ml SF inhibited all *S. aureus* growth consistently even at 72 h (Fig. 1(a.1)). Though this concentration could not inhibit the growth of other gram-negative strain. Therefore, increasing SF concentration in scaffold, it was observed that 6.4 mg/ml SF was capable to combat the *P. aeruginosa* growth completely upto 72 h but was still unable to inhibit growth of *K. pneumonia* (Fig. 1(a2)). In each of the growth curve, three different phases were observed, i.e. lag phase, exponential phase and a plateau. It was capable to inhibit complete growth of *K. pneumonia* at 8 mg/ml, which may be considered as minimum inhibitory concentration to inhibit all the gram-negative stains completely even after 72 h. Thus, this dose of 8 mg/ml was finally selected for scaffold fabrication for further use.

3.2. Characterization of PU/SF scaffold

Images of blended and immobilized PU/SF scaffolds have been depicted in Fig. 1b1 and b2 respectively. Gross morphology of the blended PU/SF scaffold is very rough and unorganized due to ran-

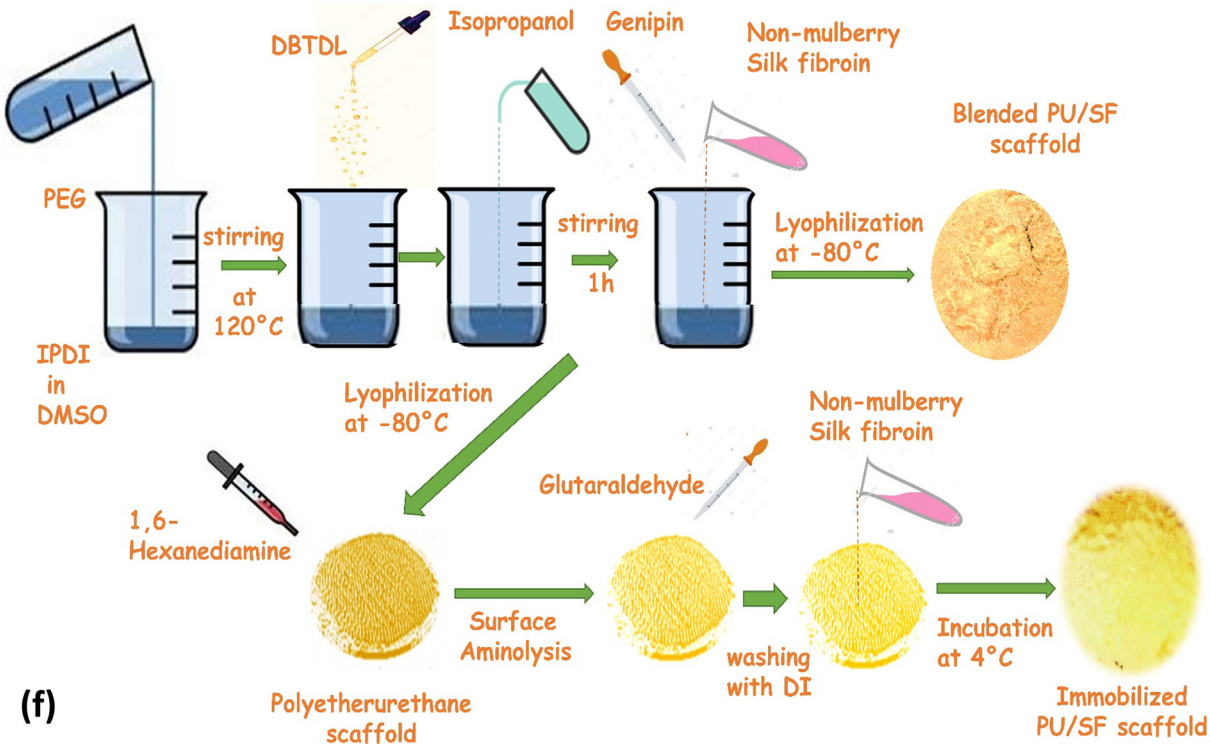

Fig. 1 (*continued*)

dom blending of PU and SF at high temperature, whereas immobilized PU/SF scaffold has smoother appearance due to immobilization of SF onto PU scaffold.

Cross sectional and top views of SEM images of blended (Fig. 2a. A–C) and immobilized (Fig. 2a. D–F) type PU/SF scaffolds showed interconnected porous architecture of the moiety. The ideal pore size for fibroblast and keratinocytic infiltration is 11 μm [37,38]. Subsequently the pore size found in the range of 22.248 ± 6.818 μm and 16.102 ± 4.802 μm for blended and immobilized PU/SF scaffolds respectively. This might be presumed that NIH3T3 cells (15 μm) would be seeded on the obtained interconnected pores. The immobilized type scaffold had rougher surface and tortuous morphology compared to that of blended variety. It may be caused by the treatment with 1,6-hexanediamine followed by glutaraldehyde what have caused the surface roughness. It is presumed that rougher the surface; greater is cellular attachment hence proliferation towards the graft. However, the exact estimate of surface roughness has been measured in atomic force microscopy for both the varieties.

AFM micrographs revealed appreciable surface roughness represented by pine like structures of the scaffolds, which is delivered by the peaks and valleys of the surface (Fig. 2b). Higher the difference between average height and valleys, more is the surface roughness. RMS roughness and Avg roughness are 534 μm, 425 μm and 464.3 μm, 377.7 μm respectively for blended and immobilized scaffolds (Table 1). Valleys are −4.181 μm, −3.974 μm and peaks are 3.819 μm and 4.014 μm. This troughs and crests aided to surface roughness enabling improved cell attachment and adhesion. Since in blended scaffolds SF is almost uniformly spread in inner architecture of PU linked by covalent bonding. Thus, SF and PU are lying at different three-dimensional planes causing more surface irregularities compared to that of immobilized one. Consequently, both RMS and Avg roughness is higher for blended scaffolds.

Water uptake is an essential property of wound dressing as it is important to absorb fluids in wound bed to fasten healing progression. Due to improved hydrophilicity of immobilized scaffold upon SF grafting, its water retaining capacity was also improved compared to that of blended type (Fig. 2c). The polar groups like —COO and —NH_2 interacted more with protic solvent water, resulting in greater water retention within porous matrix whereas due to strong covalent binding of SF and PU in blended variety, SF being strongly bound inside the matrix, not much exposed to surface causing lesser interaction with water showing lesser water retention within the scaffold. In each case, PBS is preferred over water by both type matrices as PBS is an ionic solvent due to presence of salts. Ionic salts interact more with the scaffolds resulting in higher PBS uptake. Fluid uptake was 48 ± 1.7% and 46 ± 1.3% for blended PU/SF in PBS and water respectively, whereas 60 ± 1.2%, 55 ± 1.1% for immobilized PU/SF in PBS and water respectively at 24 h. Though water uptake result in PBS of immobilized PU/SF is not significant upto first 6 h, but it was statistically significant with blended at $p \leq 0.05$ and $p \leq 0.01$ level from 9 to 24 h (Fig. 2c). In both scaffolds a steep increase in retention was found with time which may be due gradual imbibition of fluids by the surface pores.

3.3. SF and recombinant rat specific epidermal growth factor (rEGF) release profile

SF and rEGF release study were observed to investigate the release of entrapped SF from blended and immobilized type scaffolds. In cumulative release of SF in PBS (Fig. 1c), SF release was nearly equal from both blended and immobilized scaffolds but rEGF release was slightly higher by blended PU/SF over immobilized PU/SF. Cumulative SF release from both variety of PU/SF scaffold showed almost similar pattern in PBS (Fig. 1c). Immobilized PU/SF had steady increase in SF release in PBS upto 1.67 mg/ml in 15 h study whereas blended PU/SF showed initial sudden increase ranging at 8–11th h but gradually decreased after 11 h releasing maximum 0.7 mg/ml, followed by continuous release of 0.2 mg/ml from 11 h onwards to 15 h. Albeit the total SF amount released in PBS was comparatively higher in both variety PU/SF

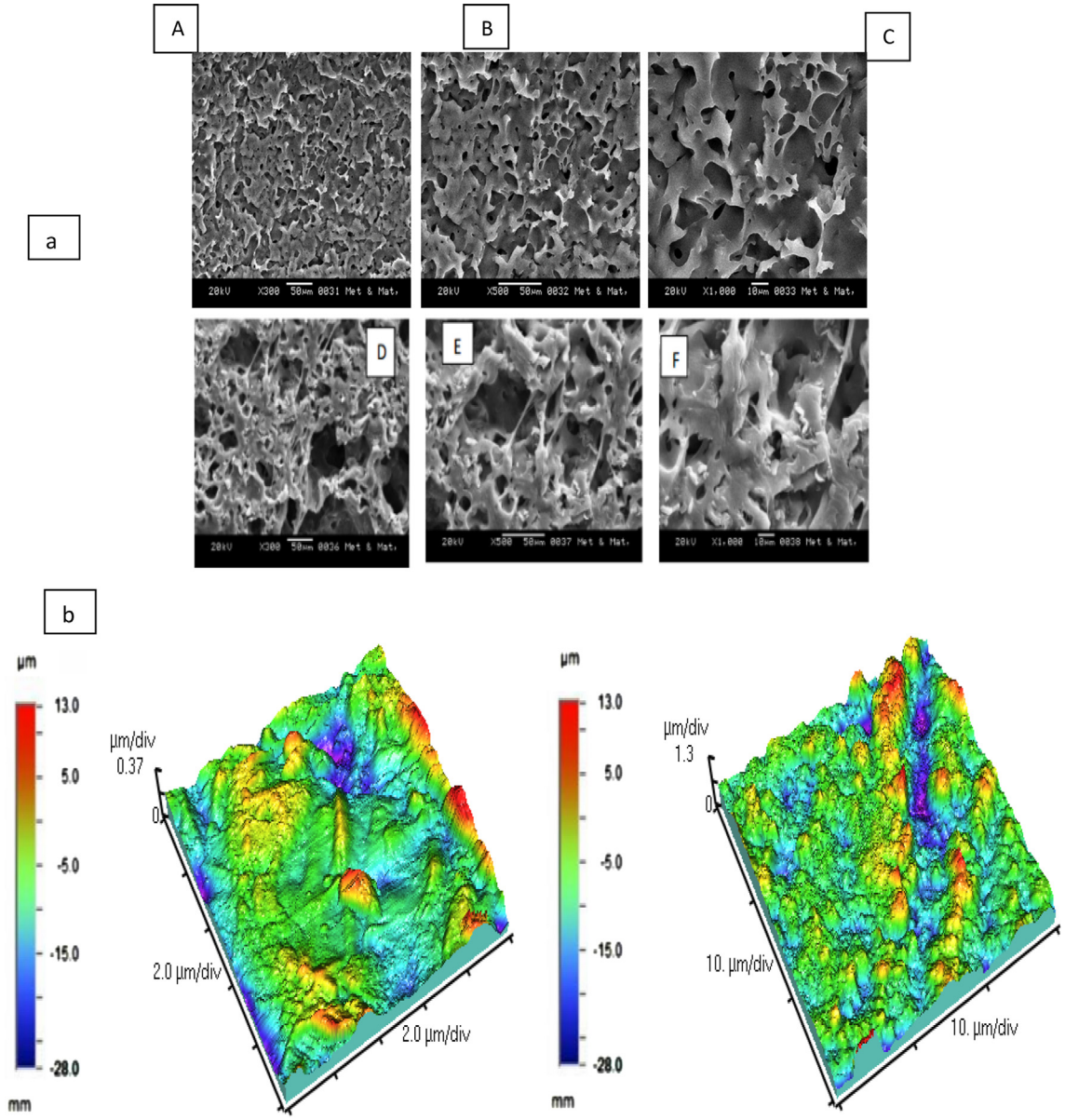

Fig. 2. (a) Scaffold morphology in Scanning electron microscopy at Blended PU/SF (A–C) 300×, 500× and 1000× magnification and Immobilized PU/SF (D–F), Scale bar (b) 3D AFM micrographs showing surface roughness of (b1.) blended PU/SF, (b2.) immobilized PU/SF (c) Water uptake profile of different scaffolds (d) Wound closure response in (d1) normal and (d2) diabetic wound by PU/SF blended (with and without EGF) and PU/SF immobilized (with and without EGF), and ActicoatTM treated wounds. Y-error bar indicates standard deviation ($n \geq 3$).

and the overall release from blended scaffold showed less and became constant after a period. Immobilized PU/SF has surface bound SF moiety which could be easily fetched by hydrogen bonds of surrounding water molecules when immersed in PBS. SF release by immobilized PU/SF was faster in PBS as PBS contains more ions which helps to fetch SF molecule, evident from the slope of linear fit curve (Fig. 1c). In contrast, since blended PU/SF had less available surface bound SF due to blending fabrication process, and mostly SF was present in core of the matrix, SF release was relatively lower for blended scaffold.

Overall release behavior of both SF and rEGF followed probable Fickian or Non Fickian kinetics. Thus, Korsmeyer-Peppas model and Higuchi model were applied on cumulative PBS release profiles of both SF and rEGF (Fig. 1d and e). In Korsmeyer and Peppas kinetic model (Fig. 1d), for immobilized PU/SF, adjusted regression (R^2) values were $R^2 = 0.9681$, 0.9835 for rEGF and SF respectively and for blended PU/SF, $R^2 = 0.9556$, 0.9842 for rEGF and SF respectively. Likewise, Residual sum of square (RSS) were RSS = 0.158 and 1.118 for rEGF and SF from immobilized PU/SF and RSS = 0.175 and 0.281 for rEGF and SF from blended PU/SF respectively. In Higuchi kinetic model, (Fig. 1e) adjusted regression was $R^2 = 0.9502$, 0.9258 for rEGF and SF from immobilized PU/SF and $R^2 = 0.9457$, 0.8767 for rEGF and SF from blended PU/SF respectively. Residual sum of square (RSS) were RSS = 0.0395 and 0.058, for rEGF and SF from immobilized PU/SF and RSS = 0.0637 and 0.0612 for blended PU/SF respectively. Therefore, Korsmeyer and Peppas model was selected as best fit model, for both SF and EGF release by two varieties of PU/SF, as evidenced by greater adjusted regression (R^2) values and higher residual sum of squares (RSS) values in Korsmeyer and Peppas model for all the cases compared to Higuchi model. The diffusion exponent value for SF release ($n = 1.75 \pm 0.066$ for blended PU/SF and $n = 2.0571 \pm 0.13$ for immobilized PU/SF);

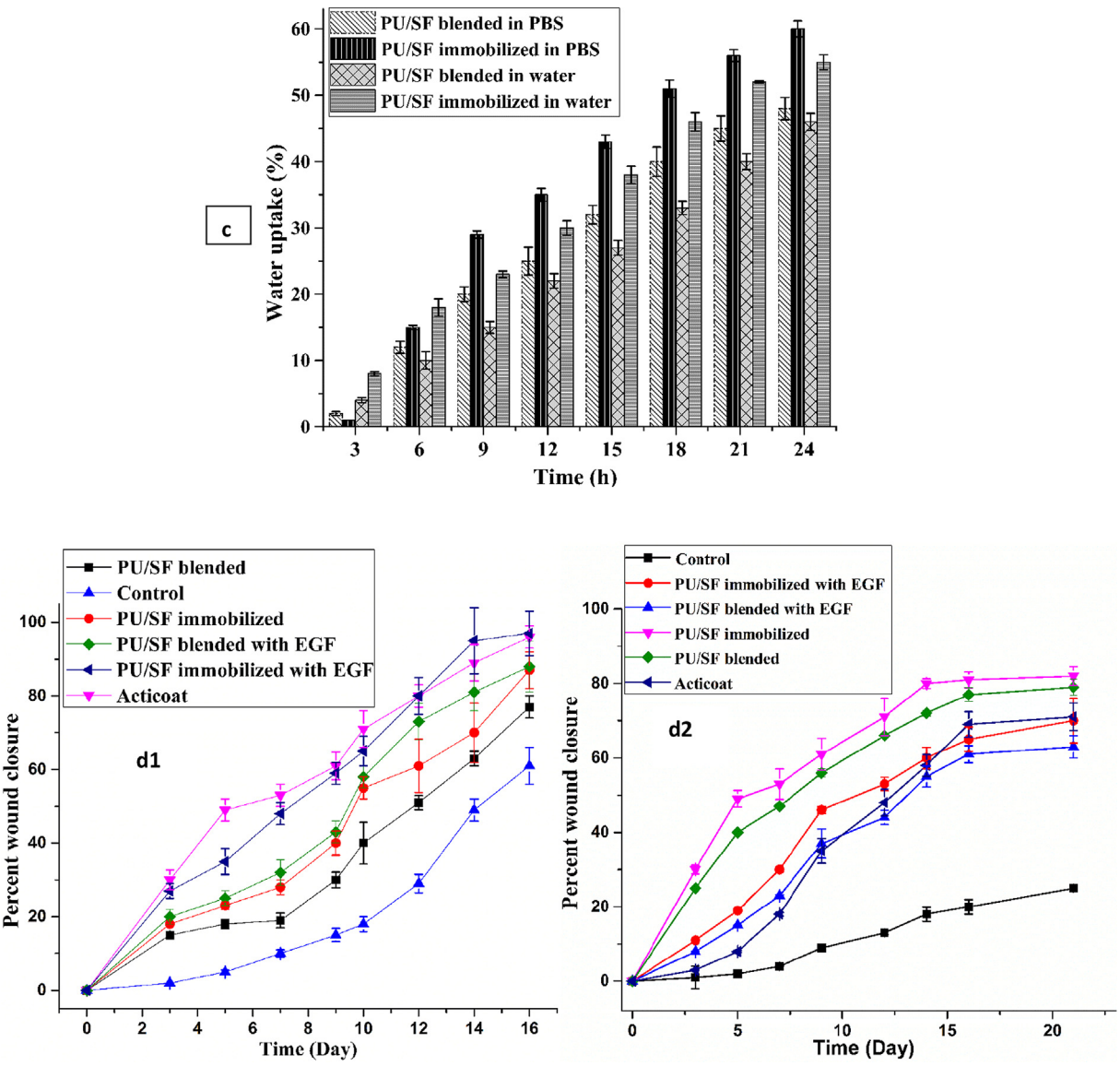

Fig. 2 (*continued*)

Table 1
Surface parameters studied in atomic force microscopy.

Sample	RMS roughness (μm)	Avg roughness (μm)	Mean ht (μm)	Median ht (μm)	Projected area (μm^2)	Surface area (μm^2)	Valley (μm)	Peak (μm)
Immobilize d PU/SF	464.3	377.7	1.615	1.725	100	113	−1.615	687
Blended PU/SF	534	425	1.389	1.357	225	276.9	−1.389	2.539

whereas diffusion exponent value for EGF release, (n = 1.354 ± 0.052 for blended PU/SF, 0.92 ± 0.05 for immobilized PU/SF) was calculated from linear plot of standard curve in the best fit Korsmeyer and Peppas Model.

3.4. Wound closure index

Gross wound healing images (Fig. 7) and rate of wound closure (Fig. 2d) by different treatment groups were applied upto 16 and 24 days for normal and diabetic burn respectively. At 16 days, Acticoat™ and rEGF incorporated PU/SF immobilized scaffold responded the best showing maximum healing percentage of 96 ± 3.1% and 97 ± 4.1% respectively at 16 days. For this treatment, surface absorbed SF, along with combined effect of rEGF and high fluid retention capacity undoubtedly contributed the best healing efficiency. Healing rate at 16 day were 77 ± 3% for blended, 61 ± 5% for control, 87 ± 3.6 for immobilized, 88%±7 for rEGF loaded blended, (Fig. 2d.1) whereas rEGF incorporated PU/SF immobilized scaffold healed completely leaving no scar behind with the secondary features of hair growth. All the treatments except the control group maintained a dry wound bed, attracting no microbial load at the wound site without changing the dressing more than twice, while Acticoat™ was changed at every 3 days interval. In diabetic wound, wound closure observed as 25 ± 0.9% for control, 70 ± 6%, 63 ± 3%,71 ± 2.7% and 82 ± 2.5% by rEGF loaded immobilized PU/SF, rEGF loaded blended PU/SF, Acticoat™, PU/SF

immobilized, 79 ± 2.1% PU/SF blended dressings respectively (Fig. 2d.2).

3.5. Wound tissue strength, blood platelet adhesion and haemocompatibility

Evaluation of wound dressings are also characterized by regenerated tissue strength. Poor tissue strength and Youngs modulus were obtained by control wound tissue which was reported by earlier study (Fig. 3a and b) [39,40]. Though Acticoat™ regenerated normal skin from full thickness burn after 3 weeks but wound strength and Youngs modulus were prominently the highest in regenerated skin repaired by rEGF containing PU/SF immobilized scaffolds (Fig. 3a and b) for both diabetic and nondiabetic wounds. Youngs modulus values of rEGF containing blended PU/SF and immobilized PU/SF treated tissue were significant ($p \leq 0.05$) between diabetic and normal wound tissue whilst wound strength of control, immobilized PU/SF and Acticoat™ treated tissues were significant ($p \leq 0.05$) between diabetic and normal wound tissue.

Since blood platelet adhesion enables to clot the hemorrhage effectively, it is a desirable quality for a wound dressing to adhere much platelets onto it. Since at various pH, amino acids from RGD sequences of non-mulberry SF dissociates, it is highly expected that ionizable groups from dissociated SF will bind to blood platelets by electrostatic interaction [41]. Blood platelet adhesion determines the heameostatic balancing capability of wound dressing scaffolds. Lactate dehydrogenase (LDH) activity is the indicator of blood platelet survival, adhered onto the scaffold. In our findings, every treatment including Acticoat™, showed significant higher LDH reactivity indicating enhanced percentage of blood platelet survival over that of surgical gauge as control. LDH reactivity attributed by rEGF containing immobilized PU/SF scaffold was the highest 5.1 mili unit/ml, which was statistically significant with control and blended PU/SF ($p \leq 0.01$), significant with blended with EGF group ($p \leq 0.05$) respectively (Fig. 3. c). It is prominent that EGF is playing crucial role in the platelet survival as rEGF loaded both blended and immobilized dressings promoted more viable platelet adhesion, even more than commercial Acticoat™.

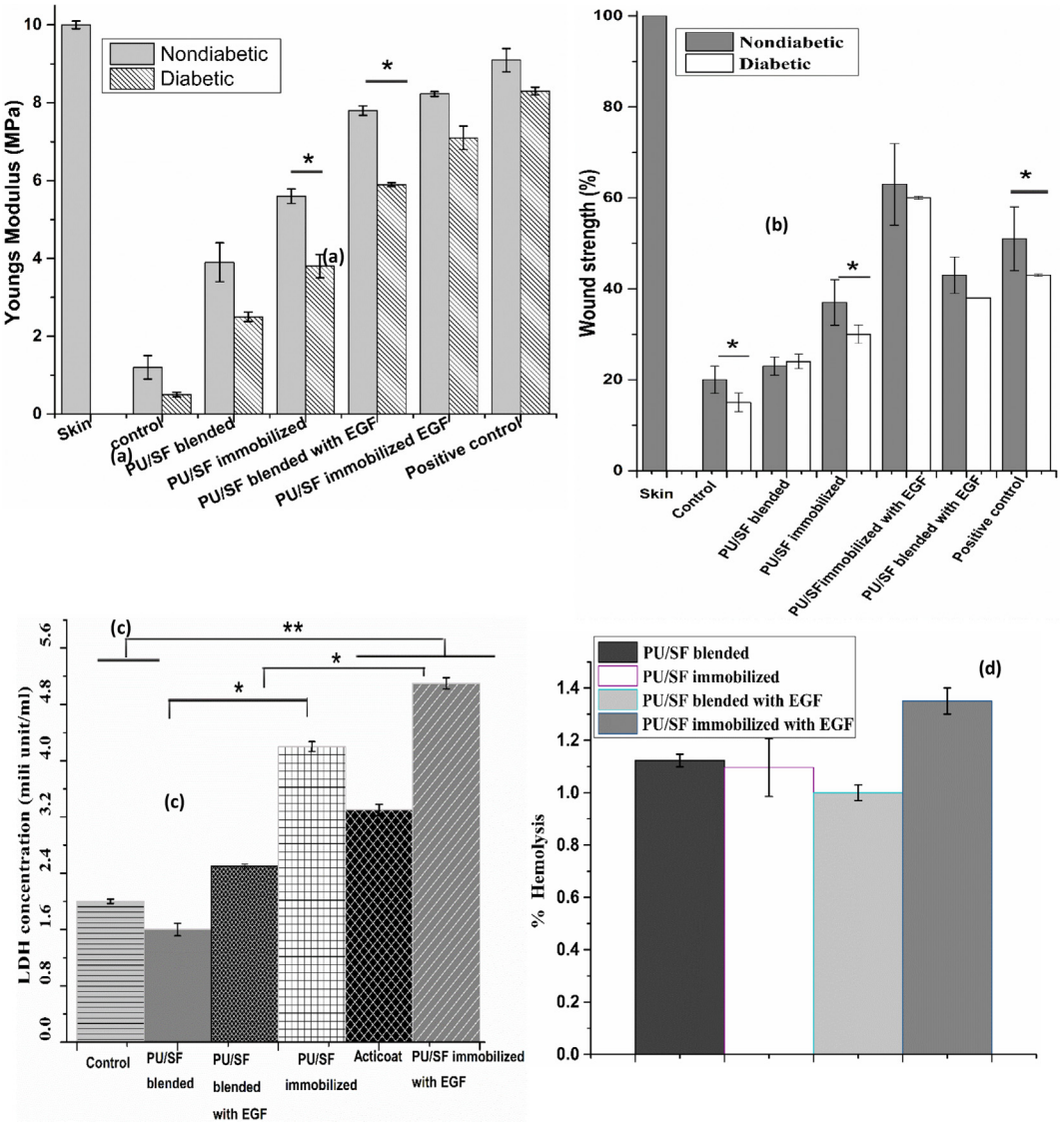

Fig. 3. (a) Young's Modulus of healed tissues by various treatments compared to normal unwounded skin (b) Wound strength of regenerated tissue by different treatments taking wound strength of unwounded skin as 100%. (c) LDH activity of adhered platelets on different scaffolds, representing haemostatic activity of composite scaffolds, control and ActicoatTM. (d) Percent Haemolysis of different composite scaffolds (*$p \leq 0.05$, **$p \leq 0.01$).

Haemocompatibility study was performed to evaluate its hemolytic tendency as wound dressing. In full thickness burn injury, wound dressing is exposed to open body fluids due to rupture of epidermis or dermis and even comes to blood contact. Hence haemocompatibility was well desired. However, Hemolytic percentage was found to be 1.123% and 1.096% for PU/SF blended and PU/SF immobilized scaffolds respectively and percent hemolysis was found to be 1.32% and 1.35% for rEGF incorporated blended PU/SF and immobilized PU/SF respectively (Fig. 3d) which lies in the non-hemolytic range of 0–2% [42]. It corroborated that rEGF did not contribute to any hemolytic effect. It can be inferred both the scaffolds are quite safe for considering as wound dressing material from haemocompatibility aspect.

3.6. Extracellular matrix development

Quantitative examination of ECM deposition of hydroxyproline, elastin and hexosamine was done to find out the role of various PU/SF based microporous dressings during wound healing process. Hydroxyproline was quantified for at every 1 week of post wounding. In non-diabetic wound, hydroxyproline level exhibited by rEGF containing immobilized mats and Acticoat™ treated wound after 7 days were statistically significant ($p \leq 0.05$) with rEGF deprived blended and immobilized PU/SF treated wounds, control, and rEGF containing blended PU/SF (Fig. 4a). At day 7 in diabetic burn, hydroxyproline level exhibited by rEGF loaded immobilized PU/SF was statistically significant with blended PU/SF without rEGF

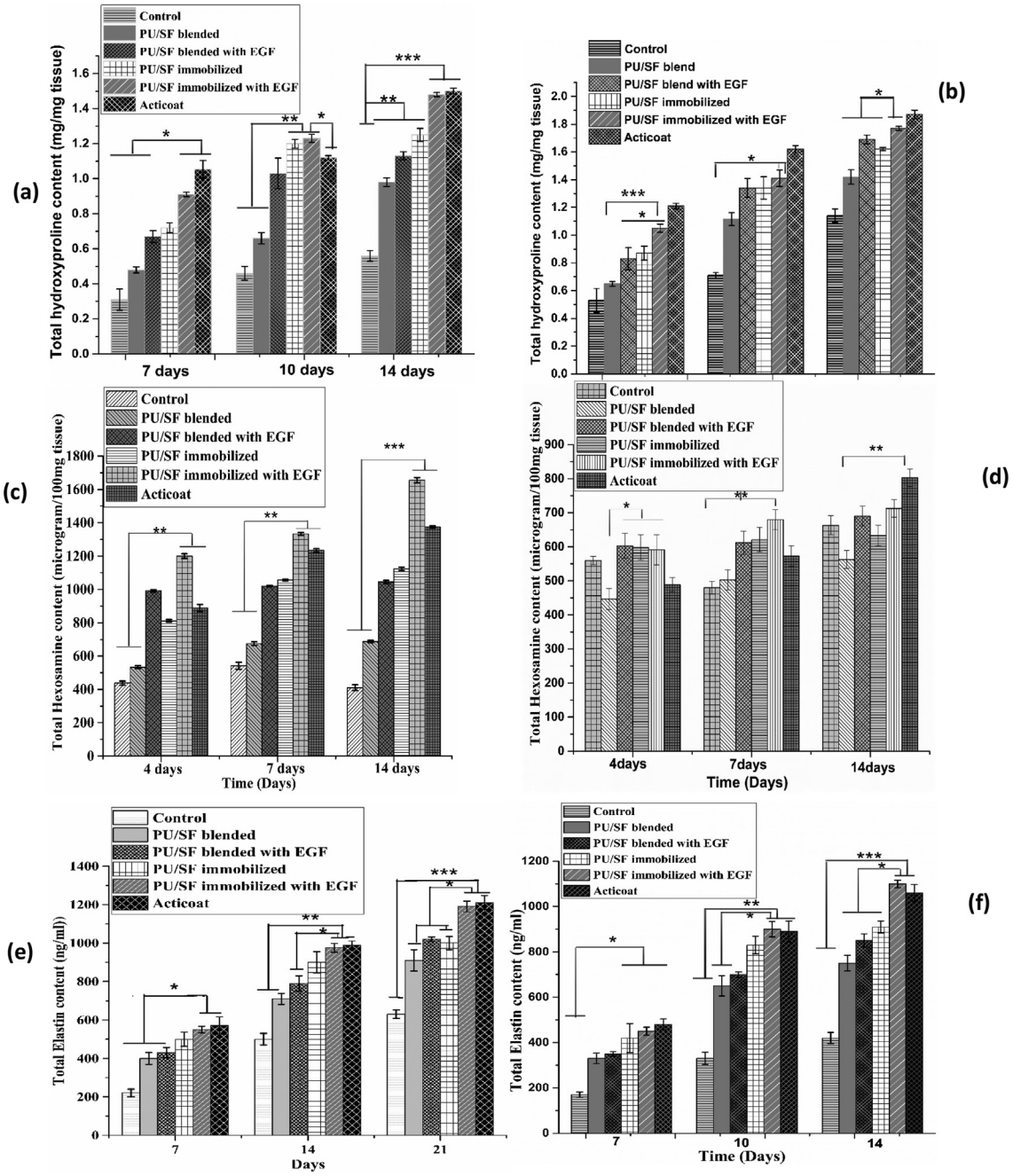

Fig. 4. Extracellular matrix composition obtained in terms of (a and b) total Hydroxyproline (c and d) total Hexosamine in normal wound and in diabetic wound at different intervals of post wounding. Y-error bar indicates standard deviation ($n \geq 3$) ($^{*}p \leq 0.05$, $^{**}p \leq 0.01$, $^{*}p \leq 0.001$).

($p \leq 0.001$), and significant with immobilized PU/SF without rEGF ($p \leq 0.05$), and rEGF containing blended PU/SF ($p \leq 0.001$) (Fig. 4b). In contrast, at 10th day of diabetic postburn, hydroxyproline released by two immobilized variety (with and without rEGF) were significant with Acticoat™ treated wound (Fig. 4 b) values were statistically significant ($p \leq 0.05$, $p \leq 0.01$) with control and blended one. By 2nd week, the data by rEGF loaded immobilized mats is significant ($p \leq 0.05$) with only PU/SF blended and immobilized varieties. In diabetic, at 14th day rEGF incorporated immobilized and Acticoat™ treated wound were significant ($p \leq 0.001$) with control and blended, blended with rEGF and only immobilized groups were significant with control ($p \leq 0.01$) respectively. Hydroxyproline release was the highest by Acticoat™ treated wound at all the intervals, but at second week, this quantity was almost equal to rEGF loaded immobilized PU/SF, differing from Acticoat™ treated wound by 100 μg only. At 7th day post burn, every group is statistically significant ($p \leq 0.05$) with each other, whereas, at 10th day, rEGF loaded immobilized PU/SF provided the highest secretion of hydroxyproline, which was also statistically significant ($p \leq 0.001$) with control, blended and blended with rEGF treatment ($p \leq 0.01$) groups and significant values with Acticoat™ ($p \leq 0.05$) treated wounds. rEGF loaded immobilized and Acticoat™ showed a prominent and significant increase in hydroxyproline deposition and this data is significant ($p \leq 0.05$) with control, blended and immobilized treated wounds. This similar performance of rEGF loaded immobilized PU/SF and Acticoat™ at 14 days, reveals that they have equal healing potential. In normal burn control wound, tissue hexosamine was of lowest concentration upto 14th day and highest and slightly greater in rEGF incorporated immobilized scaffold than that of Acticoat treated wound (Fig. 4c). This provides an insight that during repair process, this bioactive scaffold composition had encouraged sufficiently to most

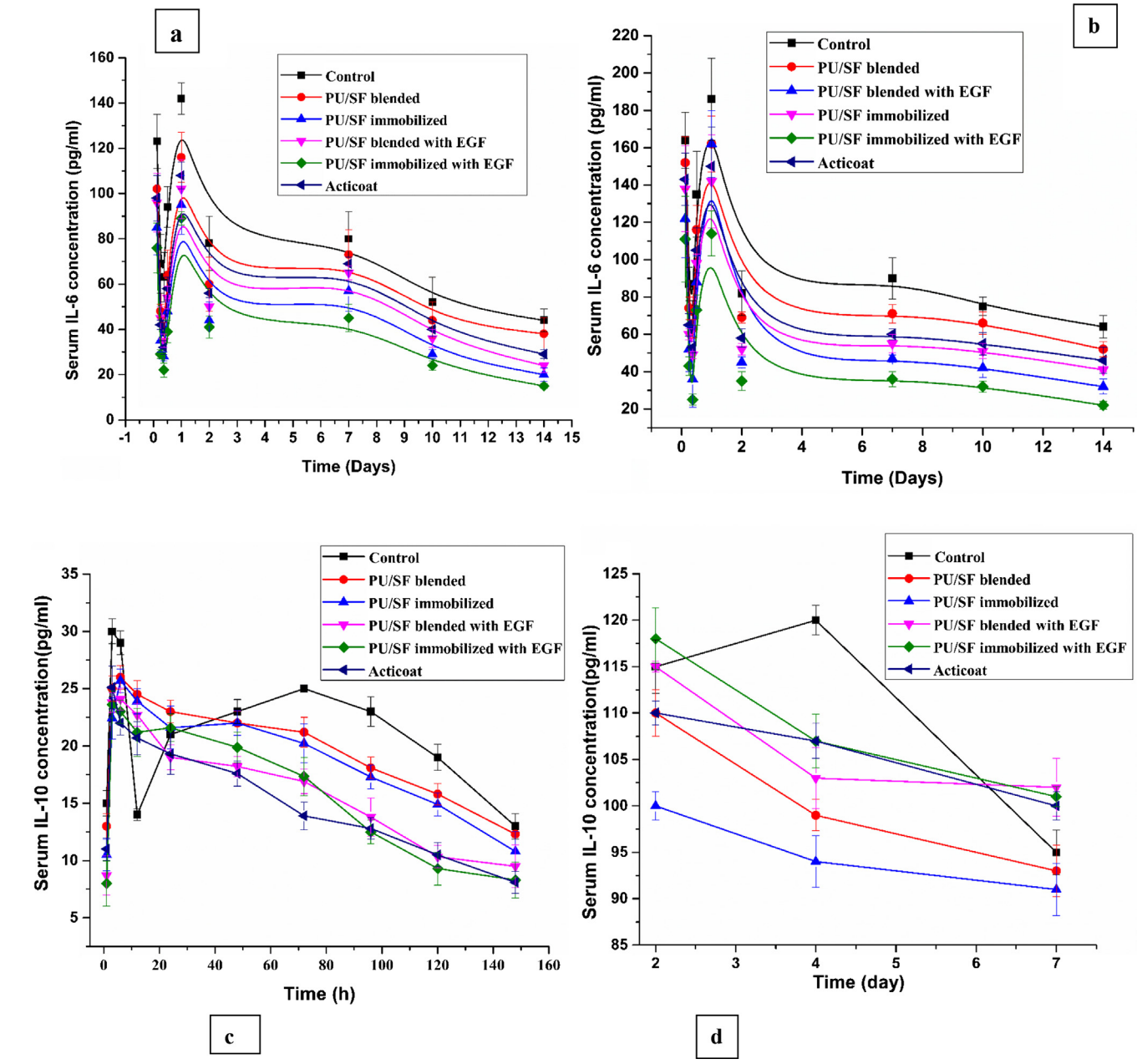

Fig. 5. (a, b). Serum IL-6 and (c, d) serum IL-10, (e, f) serum IL-8, (g, h) tissue IL-6 (i, j) tissue IL10 (k, l) tissue IL-8 concentration by PU/SF blended (with and without EGF) and PU/SF immobilized (with and without EGF) scaffold treatments in normal and diabetic wound. Y-error bar indicates standard deviation ($n \geq 3$).

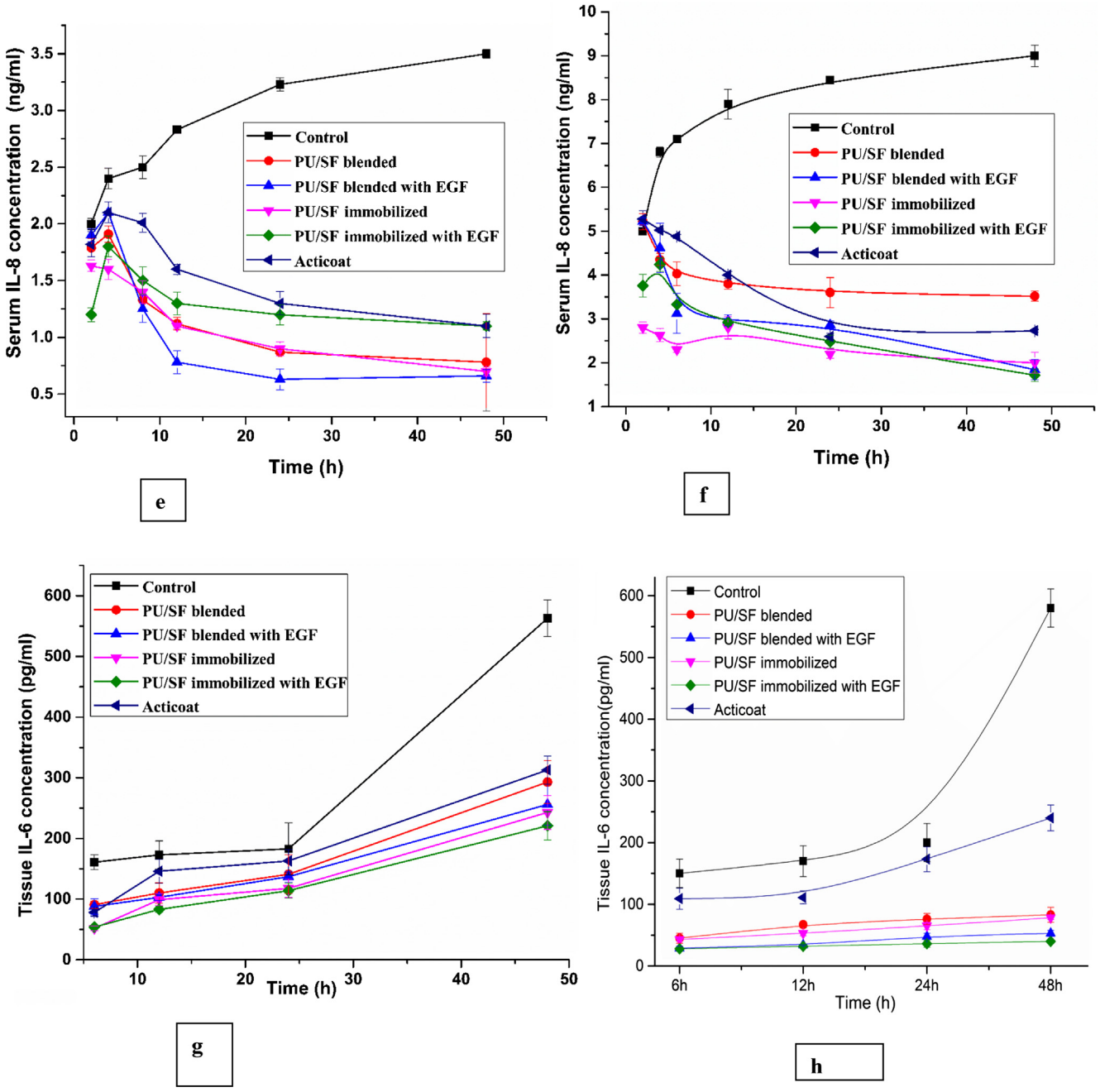

Fig. 5 (*continued*)

robust ECM deposition with effective cell-material interactions. Correlating with the fact that ECM component like hydroxyproline was deposited in a similar kinetics at biological milieu. In normal burn, by 14th day, rEGF loaded immobilized scaffold and Acticoat™ treated wound reached highest Elastin which was statistically significant at $p \leq 0.001$ level with control and $p \leq 0.05$ level with only immobilized, only blended treatments (Fig. 4e). Strikingly, in diabetic model with nearly similar results, Elastin secretion by immobilized with rEGF and Acticoat™ was significant ($p \leq 0.001$) and ($p \leq 0.05$) with blended, blended with rEGF and immobilized one (Fig. 4f). Consistent increase with least standard deviation of rEGF loaded immobilized PU/SF at all intervals suggests its highest efficiency among all the groups. For Hexosamine, 20.9 mg is the standard value of skin tissue hexosamine in normal rat [43]. For all the treatment groups in burn model, there is a similar elevation from 7th to 10th day indicating that all the treatment groups were effective enough. However, the most efficiency was exhibited by the rEGF loaded immobilized variety at both 10th and 14th day.

3.7. Characterization of inflammatory cytokine analysis

In chronic nonhealing burn, oxidative stress causes sudden elevation in inflammatory cytokines and immunoglobulins like IL-6, IL-8, IL-10 [44]. Tissue IL-6 values were 88.7 mg/dl and 57.3 mg/dl and serum IL-6 values were 3.4 mg/dl and 21.58 mg/dl as obtained in nondiabetic and diabetic unburnt normal skin (sham) tissue. This tentatively matches with the earlier reported study [45]. Tissue IL-10 values were 100 pg/ml for nondiabetic and 600–630 pg/ml for diabetic unburnt skin (sham) respectively. Serum IL-10 values were obtained 6 pg/ml and 90 pg/ml for nondi-

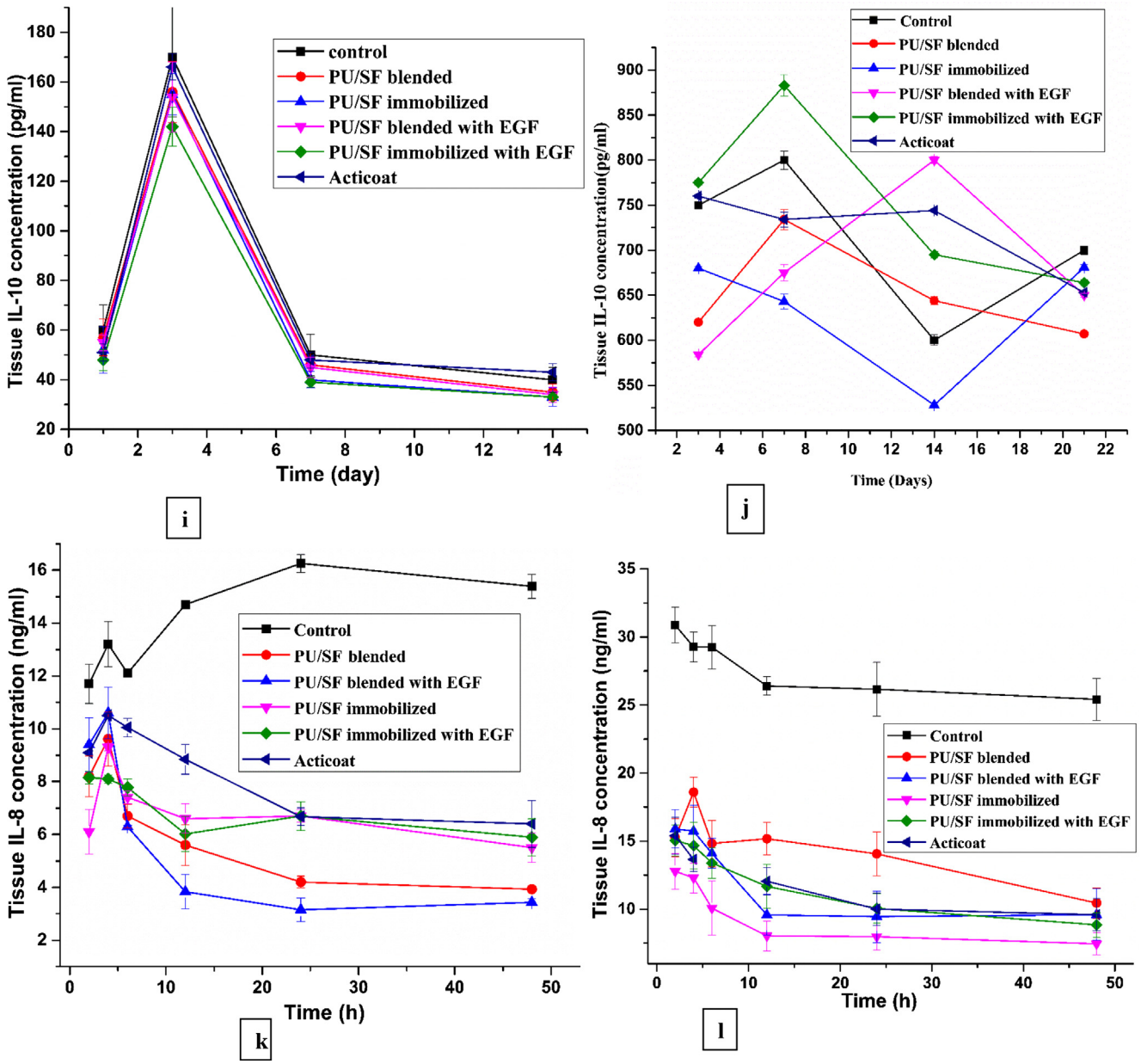

Fig. 5 (*continued*)

abetic and diabetic unburnt animal's serum (sham) by ELISA. After burn, raised serum IL-6 level was restored by 2 weeks by control (surgical gauge treated groups), but when they were treated with different PU/SF scaffolds and Acticoat™, their normal level of IL-6 were restored faster (Fig. 7) than control (surgical gauge treated groups). This recovery by PU/SF mats was faster in non-diabetic burn than that of hyperglycemic burn. In contrast, serum IL-10 level was abruptly increased by control groups within one day of burn, whereas this increase was characteristically controlled by immobilized and blended PU/SF from beginning. Though the scaffold treated group also showed sudden increase of serum and tissue IL-10 level, but gradually they restored to normal range within one week, while control and Acticoat™ treated groups were unable to restore to normal range within a week.

The serum IL-6 value at 3 h post burn by control wounds in normal burn raised to 123 pg/ml and 164 pg/ml respectively (Fig. 5 (a)). In hyperglycemic burn, the serum IL-6 values were recorded as 96 pg/ml, 102 pg/ml, 85 pg/ml, 76 pg/ml, 98 pg/ml at 3 h post-burn in rEGF loaded blended, blended, immobilized, rEGF loaded immobilized PU/SF treated and Acticoat™ treated wounds respectively (Fig. 5(b)). In normal burn, though serum IL-6 values between different groups were statistically not significant ($p \leq 0.05$) with each other but tissue IL-6 values of rEGF loaded matrices were significant with control ($p \leq 0.1$). In diabetic group, lowest serum IL-6 level, (111 pg/ml, at 3 h) was observed by immobilized PU/SF (Fig. 5(b)), while IL-6 values were 143 pg/ml and 138 pg/ml by Acticoat™ and rEGF incorporated immobilized PU/SF treated wounds respectively. Blended PU/SF without rEGF was 122 ± 23 pg/ml at 3 h in diabetic burn indicating rEGF might not have significant role in restoring the serum IL-6 level. In hyperglycemia, rEGF had played profuse role in tissue cytokine restoration more than that of serum. This hypothesis complied with the results of tissue IL-6 level (Fig. 5(g) and (h)) in diabetic burn. In wound tissue, IL-6 restoration at 48 h by rEGF incorporated immobilized and blended PU/SF composite scaffolds (221 ± 23 pg/ml) were much prominent (Fig. 5(h)) compared to the response by

rEGF deprived groups, Acticoat™ (313 ± 18 pg/ml) treated wound and control (563 ± 30 pg/ml) in diabetic group. In contrast, diabetic serum IL-6 levels responded differently at 48 h; rEGF deprived immobilized group restored highest (35 ± 5 pg/ml), compared to rEGF loaded immobilized PU/SF (52 ± 5 pg/ml), control (82 ± 12 pg/ml) and Acticoat™ (58 ± 8 pg/ml) respectively (Fig. 5 (b)). At 14 days, diabetic serum IL-6 level was retained to 22 pg/ml, 46 pg/ml, 64 pg/ml by rEGF deprived immobilized PU/SF group, Acticoat™ and control respectively (Fig. 5(b)). However, normal serum IL-6 level was restored back to 29 pg/ml by Acticoat, 15 pg/ml by rEGF loaded PU/SF treatment, 44 pg/ml by control (Fig. 5(a)) respectively. Overall it was interpreted that serum IL-6 restored back earlier compared to that of tissue IL-6 due to wound vicinity affected the tissue greater extent. In nondiabetic burn, increase in serum IL-6 due to oxidative stress was resisted by rEGF loaded blended and immobilized PU/SF groups (Fig. 5(a)). Serum IL-6 and IL-10 profile was similar in diabetic wound, as in both cases, rEGF treated groups was less efficient compared to rEGF deprived groups. Likewise, at 2 days diabetic post-burn, serum IL-10 level, exhibited by control, Acticoat™ and rEGF deprived immobilized PU/SF groups were 110 ± 7.6 pg/ml, 116 ± 4.3 pg/ml and 98 ± 3.1 pg/ml (Fig. 5(d)). Increase in tissue IL-10 level was highly resisted by both immobilized groups at greater extent than Acticoat treatment in non-diabetic wound (Fig. 5(i)). This enhanced restoration of IL-6 level and strong resistance to elevation of IL-10 level by PU/SF mats have a definite correlation with its antioxidant potential. Diabetic tissue IL-10 level was restored maximum by blended group followed by rEGF loaded blended and immobilized and Acticoat treated groups (Fig. 5(j)). Likewise, IL-8 profile both in tissue and serum were elevated in diabetic burn compared to normal but faster restoration was confirmed by both the rEGF treated and untreated PU/SF immobilized groups in diabetes with respect to control (Fig. 5(e), (f), (k), and (l)).

3.8. Western blotting and zymography

Crude protein samples and expression of E-cadherin was examined for both normal and diabetic wounds after 14 days of treatment groups and control by protein slab gel electrophoresis and western blotting, respectively (Fig. 6(a) and (b)). In normal wound, E-cadherin expression was gradually increasing from PU/SF blended to rEGF incorporated immobilized PU/SF and Acticoat which also complied with gross wound healing results. Among the groups, control tissue did not express E-cadherin at all in either case of diabetic or normal wound of 14 days postburn whereas in PU/SF blended, PU/SF immobilized, rEGF containing blended PU/SF and rEGF containing immobilized PU/SF treated tissues had shown gradual significant expression. rEGF loaded treatments showed markedly higher E-cadherin expression in normal wound. However, in diabetic wound, this finding reversed as the intensity of expression by rEGF loaded blended PU/SF and rEGF loaded immobilized scaffolds were lesser compared to rEGF deprived groups (Fig. 6(b)). This reflected, rEGF deprived PU/SF treatment groups expressed more E-cadherin in diabetic burn and rEGF containing PU/SF groups expressed higher level of E-cadherin in normal burn. However overall E-cadherin expression was more prominent in nondiabetic wound as compared to diabetic wound [46]. In contrast to E-cadherin expression in western blot, MMP 9 was more intensely found in rEGF loaded PU/SF groups both in normal and diabetic burn compared to rEGF deprived PU/SF groups in zymographic study (Fig. 6(c)). This reverse response in diabetic burn by EGF incorporated PU/SF groups resulting in lesser expression of E-Cadherin in western blot and intense expression of MMP 9 in zymography could be attributed to the fact that EGF enhances matrix metalloproteinase (MMP 9) level which is responsible for raising the matrix degrading proteases [47]. This rise in MMP 9

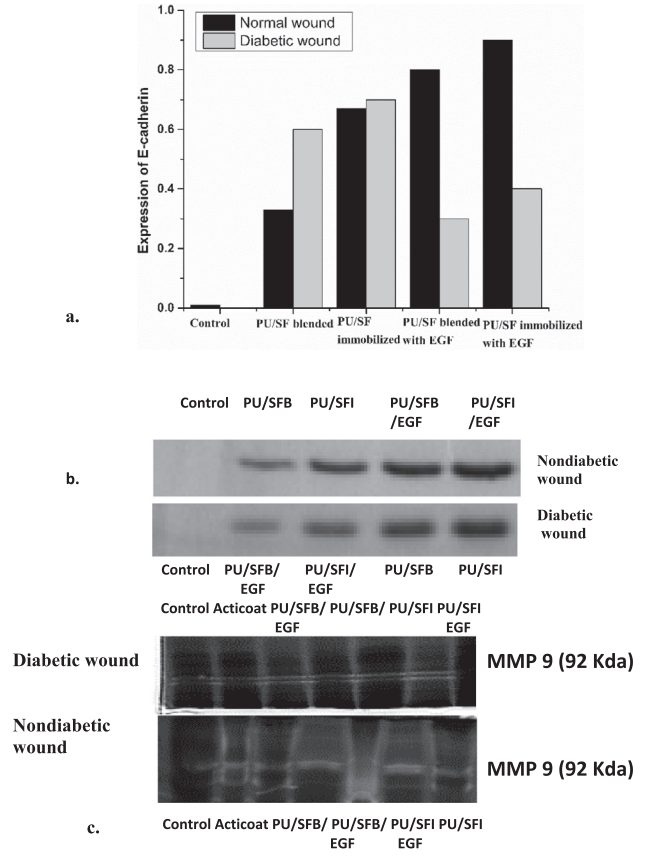

Fig. 6. (a). Fold change of E-cadherin protein expression following western blot of control and four dressings treated wound samples. (b) Representative western blot image of E-cadherin protein expression. (c) Expression of MMP9 in gelatin zymography in diabetic and normal wound tissue treated by control, different scaffold groups and Acticoat in diabetic and non-diabetic wounds.

in turn lowers E-cadherin expression intensity [48]. Gelatin zymography analysis of granulation tissue showed enhanced MMP-9 expression by all the treatment groups as compared with controls. During onset of maturation phase of wound healing, MMP-9 plays crucial role in remodeling extracellular matrix and collagenization. Gelatin zymography revealed more intense expression of MMP-9 in EGF-treated PU/SF group, specially immobilized PU/SF groups, suggesting that these treatment groups might be aiding maximum in matrix remodeling phase.

3.9. Histomorphology evaluation

The ultimate phase of wound healing is maturation phase which involves re-modelling of matrix components evident in histological study. H & E staining exhibited gradual typical cellular accumulation tendencies at four basic different stages of wound healing, i.e. hemostasis, inflammatory, proliferative and maturation phases. H & E response of each treatments including control and Acticoat™ treated diabetic and nondiabetic wounds were scored at every time points based on different parameters of wound [Tables 2 and 3]. In diabetic groups at 3rd day, complete dermal rupture was observed (Fig. 8A(a)–(f)) and at 7th day, fat cells embedded with multiple nucleus, lymphocytic infiltration and onset of granulation tissue was predominantly observed in rEGF deprived blended PU/SF (Fig. 8A(h)), rEGF deprived immobilized PU/SF (Fig. 8A(i)) treated groups exhibiting highest scoring whereas escher formation, prevalence of necrosis and lesser granulation tissue was seen at 7th day control (Fig. 8A(g)), blended and

Table 2
Parameters of wound scoring at different healing stages from 3 days to 21 days post burn.

Scores	Parameters
0–1	There was loss of dermal component, lot of necrotic tissue, lymphocytic infiltration hyperemia in hypoderm
1–2	There was necrotic tissue, inflammatory cells and onset of new blood vessel formation and fibroblasts
2–3	There was fibroblast proliferation, accumulation of collagen, new blood vessel formation and inflammatory cells
3–4	There was proliferation of fibroblast, accumulation of collagen, new blood vessel appearance, few inflammatory cells and newly formed epithelial tissue
4–5	There was marked epithelialization and scar tissue formation
5–6	There was complete epithelialization, regeneration of hair follicles, sebaceous gland and scar tissue of the burn

immobilized with rEGF containing group (Fig. 8A(j) and (k)) and Acticoat™ (Fig. 8A(l)) treated groups indicating slower healing rate where proliferation phase was yet to begin. At 10 days post wounding, though Acicoat™ treated groups showed response of proliferation phase (Fig. 8A(n)–(r)) but PU/SF scaffold treated groups depicted well-formed matrix of dermal structures and different strata of epidermal layers along with budding of collagens and angiogenic points. Wound contraction was evident as thin epithelial layer progressing towards central wound area was quite prominent at 18th day in rEGF deprived blended and immobilized PU/SF scaffold (Fig. 8A(t) and (u)) treatments, whereas onset of epidermal stratification was observed by rEGF containing blended (Fig. 8A(v)) and rEGF containing immobilized PU/SF (Fig. 8A(w)) groups at day 21. Wounds were devoid of epidermis at 21st day in control ((Fig. 8A(s)) and incomplete epidermis formation by Acticoat™ treatment (Fig. 8A(x)) evidenced delayed diabetic wound healing.

Like diabetic group, nondiabetic control also showed complete dermal rupture (Fig. 8B(a)–(f)) in all the groups at 3 days, but in all treatment groups, including Acticoat™, onset of necrotic tissue, inflammatory cells and fibroblasts accumulation were started from 3 days (Fig. 8B(b)–(f)), scored between 1.3 and 2.3. At 7th day, few inflammatory cells were seen in control (Fig. 8B(g)) and almost no inflammatory cells like macrophage, dendritic cells etc. was visible in rEGF incorporated PU/SF varieties and Acticoat treated groups (Fig. 8B(j)–(l)). In no groups, acute inflammation was observed indicating nontoxic nature of the patches. Granulation tissue started emerging in the wound within 7 days post injury by all four treatments including Acticoat™ (Fig. 8B(h)–(k) and (l)). In 7 days, cardinal sign of healing, i.e. onset of neovascularization and accumulation of collagen were more pronounced in rEGF loaded blended (Fig. 8B(j)), rEGF loaded immobilized groups (Fig. 8B(k)) and Acticoat™ (Fig. 8B(l)) treated groups compared to control (Fig. 8B(g)) and either of rEGF deprived PU/SF varieties (Fig. 8B (h) and (i)). Inflammatory cells were absent but fibroblast and keratinocyte recruitment, scar formation prevailed at 10 days in all the blended and immobilized groups including Acticoat™ (Fig. 8B (n)–(q) and (r)) For rEGF loaded treatments (Fig. 8B(p) and (q)) and Acticoat™ (Fig. 8B(r)) treated groups, partial re-epithelialization started with well patterned reconstructed dermis in different stratum with developed epithelial lining in contrast to control (Fig. 8B(m)) where it was yet to restore the epidermis. At 14th day, rEGF deprived immobilized group (Fig. 8B(u)) (score 5.3), rEGF loaded blended (Fig. 8B(v)) (score 5.4) and rEGF loaded immobilized PU/SF (Fig. 8B(w)) treated wound (score 5.6), Acticoat™ treated wound (Fig. 8B(x)) (score 5.2) showed typical secondary features like sebaceous gland, hair follicle, nerves and sweat gland formation. Collagenization orientation and re-epithelialization alignment of Acticoat™ treated wound resulted in comparative less scoring than that of rEGF loaded immobilized PU/SF groups. In terms of considerable fibroblast recruitment, decreasing macrophages and neutrophil population, granulation tissue and aligned re-epithelialization, rEGF loaded cellular PU/SF immobilized matrix scored highest at 14 days in normal wound and cellular PU/SF immobilized matrix without rEGF scored the highest at 21 days for hyperglycemic wound [49].

MT staining revealed collagen deposition in separate pattern in each treatment for diabetic and nondiabetic groups. The pattern of mature (Fig. 9B(t)–(w)) tissue clearly indicated thicker collagen accumulation in immobilized, rEGF incorporated blended and rEGF incorporated immobilized PU/SF hybrid mats treated wounds evidenced by dispersed blue stain when compared to blended PU/SF without rEGF (Fig. 9B(t)), control (Fig. 9B(s)), and Acticoat™ treated wound (Fig. 9A (x)) in nondiabetic wound. This implies rEGF loaded blended and rEGF loaded immobilized PU/SF treatment helped to restore the dermal architecture by faster re-epithelialization and higher recruitment of fibroblasts. These findings also corroborated the enhanced deposition of hydroxyproline at 14 days which supported promising ECM development. In contrast, in diabetic wound control, blended PU/SF and Acticoat™ treated wounds resulted in immature, shattered, thin, and scanty collagen fibers lining in hyperglycemic wound at 21 days. Though rEGF loaded treatments scored less in H&E staining in diabetic wound, but mature collagenization might be contributed by the stimulatory effect of rEGF.

3.10. Immunohistochemical evaluation

The tissue sections were investigated by immunohistochemical studies for observing the characteristic marker expression of hemostatic stage (anti-smooth muscle actin), neovascularization (anti-CD31), proliferative phase (anti-Ki67), maturation phase (anti-Col III) of wound healing. Onset of neovascularization was supported by expression of angiogenic marker CD31 at day 7 post wounding. EGF loaded immobilized PU/SF and EGF loaded blended PU/SF group (Fig. 10A(b) and (c)) showed highest expression of CD31 and alignment of thinner blood vessels leading to granulation tissue development. Successful neovascularization in all treatment groups may be partially credited to microporous interconnected architecture of scaffold which indirectly con-

Table 3
Scores of control, PU/Sf blended and immobilized (with and without EGF; four treatment groups) scaffolds, Acticoat in normal and hyperglycemic wound at at different healing stages from 3 days to 21 days post burn.

Groups	Scores of non-diabetic groups				Scores of diabetic groups			
	3 day	7 day	10 day	14 day	3 days	7 days	10 days	21 days
Control	0.5	1	2	3.5	0	1.1	1.8	2
Blended PU/SF	1.4	1.9	3.1	5.1	1.3	1.3	2.5	3
Immobilized PU/SF	1.6	2.4	4.2	5.3	1.7	1.9	2.4	3.9
Blended PU/SF with EGF	1.7	2.7	4.2	5.4	1.1	2.2	4	5.1
Immobilized PU/SF with EGF	1.8	2.8	5.1	5.6	1.3	2.4	4.7	5.3
Acticoat™ treated	2.3	2.8	5.0	5.2	1.6	3.2	4.9	5.3

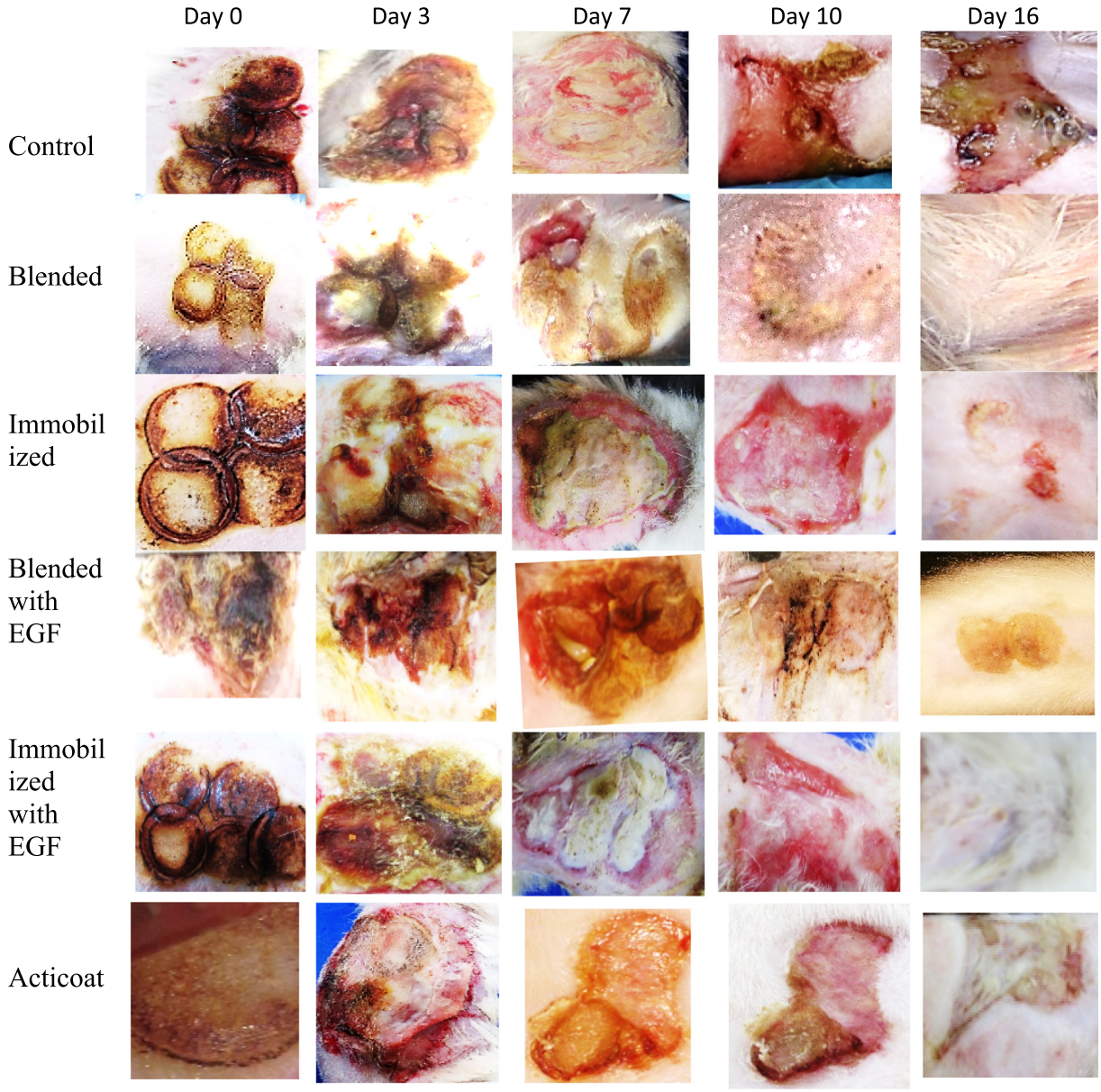

Fig. 7A. Optical images of gradual wound healing response of different treatments, control and Acticoat™ as positive control at different intervals of post burn in normal wound.

tributed to granulation and epithelial repair by promoting blood vessel formation [50,51]. In diabetic wound, EGF incorporated blended and immobilized PU/SF groups including Acticoat (Fig. 10B(b), (c), and (f)) CD-31 presented with highly immature tortuous and densely packed vessels for control groups whereas EGF deprived immobilized PU/SF group (Fig. 10B(d) and (e)) revealed thinner blood vessel development. The keratinocytic infiltration was quantified by anti-Ki-67 (nucleus) antibody at 7 days post wounding. Significant differences were exhibited by basal keratinocytes in EGF incorporated immobilized PU/SF and Acticoat™ treated nondiabetic wounds (Fig. 10A(n), (o), and (r)). In control group, magnitude of Ki-67 was mostly found in basal part of epidermis. An increase in prevalence of Ki-67+ epidermal cells were observed among tissue treated by EGF containing immobilized PU/SF and EGF deprived blended and immobilized PU/SF groups in diabetic burn (Fig. 10B(o), (p), and (q)). Unlike other histochemical response of diabetic wound tissue, proliferative response was greater by EGF containing immobilized PU/SF treated wound (Fig. 10B(o)). Magnitude of keratinocytic infiltration differed by Acticoat treated groups between diabetic and nondiabetic wound significantly (Figs. 10A(r) and 10B(r)). At 14 days post burn, most of the EGF containing blended PU/SF and EGF deprived immobilized PU/SF treated normal wound exhibited deep fete ridges (Fig. 10A(n) and (q)). Number of Ki-67 expressing cells were significantly less in Acticoat treated (Fig. 10B(r)) and EGF-treated diabetic wound (Fig. 10B(n) and (o)) sites. Non-diabetic groups retained greater Ki67+ cells as compared to all respective treatment groups in diabetic wound (Figs. 10A(m)–(r), 10B(m)–(r)). Epidermis of wound tissue, treated by rEGF containing PU/SF showed distinctively different patterns of Ki-67 reactivity compared to epidermis of wound tissue, treated by rEGF deprived PU/SF and Acticoat™ groups in both diabetic and nondiabetic wound. Epidermis was found parakeratotic and characterized by higher magnitude of Ki-67 expressing cells in basal layer for both type of immobilized PU/SF (with and without rEGF) treated wounds (Fig. 10B(o) and (q)). Most significantly, Ki-67 abundance was not limited to basal

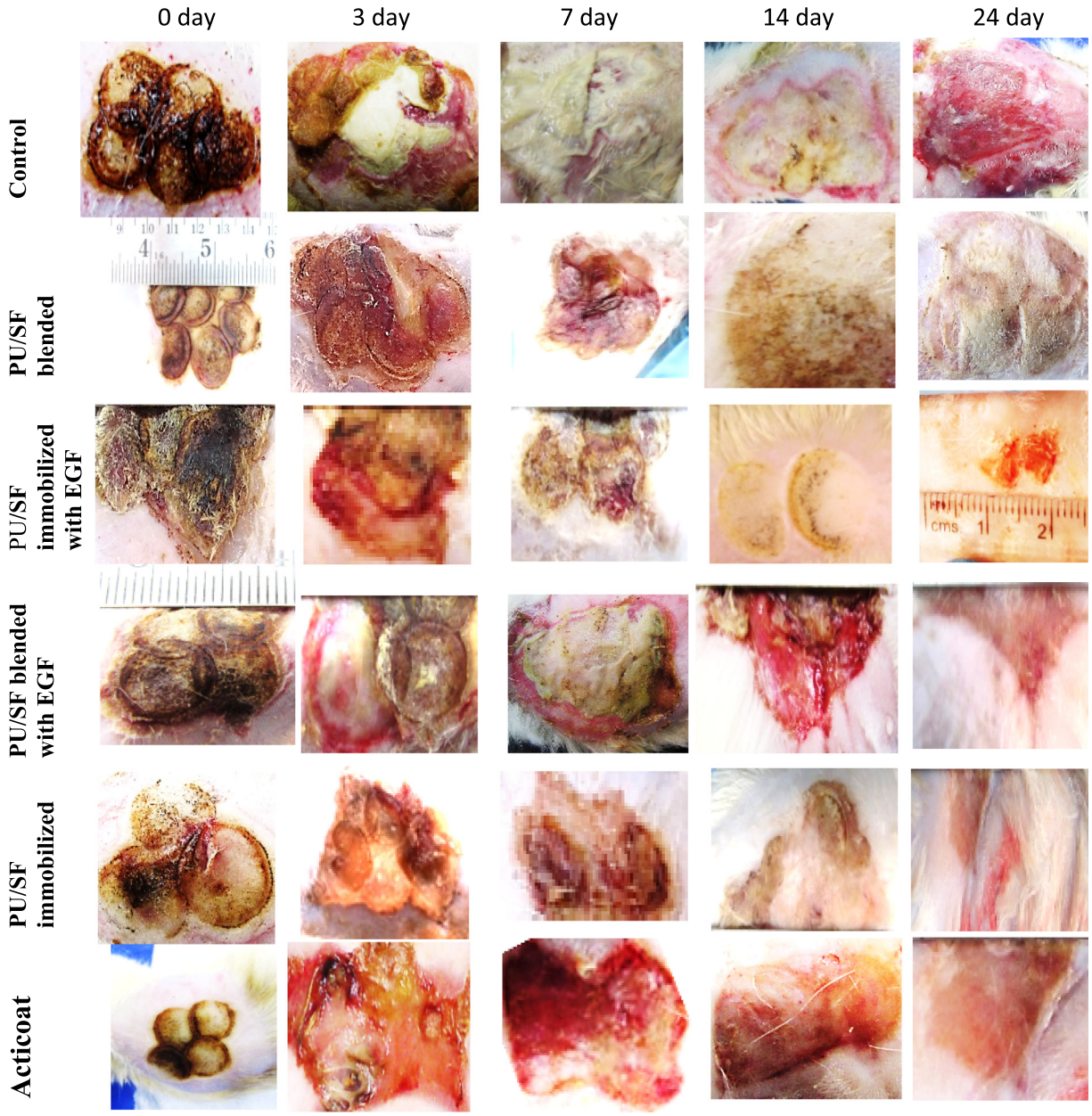

Fig. 7B. Optical images of gradual wound healing response of different treatments, control and Acticoat™ as positive control at different intervals of post burn in diabetic wound.

part, but it was evident in the supra-basal layer in treatment groups of normal wounds (Fig. 10A(h), (i), and (k)). On the contrary, Ki-67 expression was relatively less abundant and precisely confined in single basal region in the epidermis of wound sites treated by blended PU/SF and Acticoat™ (Fig. 10A(p) and (r)). These findings suggest that both EGF incorporated and EGF deprived immobilized PU/SF dressings induce early persistent proliferative response on epidermal remodelling compared to the other groups. After 14 days, re-epithelialization was confirmed by anti-Col III antibodies in EGF treated PU/SF and Acticoat™ treated groups (Fig. 10A(h), (i), and (l)) as clear stratified epithelial layer formation was evident in nondiabetic groups. A thin epithelium formation was ensured by little expression of anti-Col III in rEGF deprived blended and immobilized PU/SF treated wounds (Fig. 10A(j) and (k)). In diabetic wound control, anti-Col III expression was almost absent (Fig. 10B(g)) showing poor epithelialization in H & E staining. In hyperglycemic condition, though Col III expression prevailed more in rEGF deprived PU/SF groups treated wounds (Fig. 10B(j) and (k)) but rEGF incorporated PU/SF treated tissue (Fig. 10B(h) and (i)) also showed higher deposition of Col III than that of Acticoat treated wound which was further supported by MT staining. At 10 days post burn, cytoplasmic staining of extracellular matrix was characterized by anti-alpha sma antibody for myofibroblast differentiation [52]. Tubular complexes that were detected by anti- alpha sma antibody in the ECM of epidermis at the margin of nondiabetic wound, prevailed in wound tissues treated by rEGF loaded blended PU/SF, rEGF loaded immobilized PU/SF and Acticoat (Fig. 10A(t), (u), and (x)). Anti-alpha sma was detected in very well pattern in basal epidermal layer by rEGF loaded immobilized PU/SF and rEGF loaded blended PU/SF groups compared to Acticoat™ treated groups. This banding pattern suggested smooth muscle actin expression by rEGF loaded immobilized PU/SF was caused by synergistic effect of enhanced SF and rEGF release from immobilized matrix. This strong appearance of alpha sma was

Table 4
Blood glucose levels in different groups after administration of streptozotocin (STZ) injection (n = 6). Values are expressed as mean ± S.E.

Group	Days					
	Day 0 (STZ injected) (mg/dl)	Day 3 Post STZ administration (mg/dl)	Day 3 Postburn (mg/dl)	Day 7 Postburn (mg/dl)	Day 14 Postburn (mg/dl)	Day 21 Postburn (mg/dl)
Control	95.07 ± 8	540 ± 15	450 ± 34	250 ± 23	290 ± 9	221 ± 48
Blended	86 ± 18	530 ± 22	480 ± 42	412 ± 32	341 ± 12	225 ± 12
Immobil ized	106 ± 38	510 ± 26	435 ± 33	393 ± 53	330 ± 34	223 ± 43

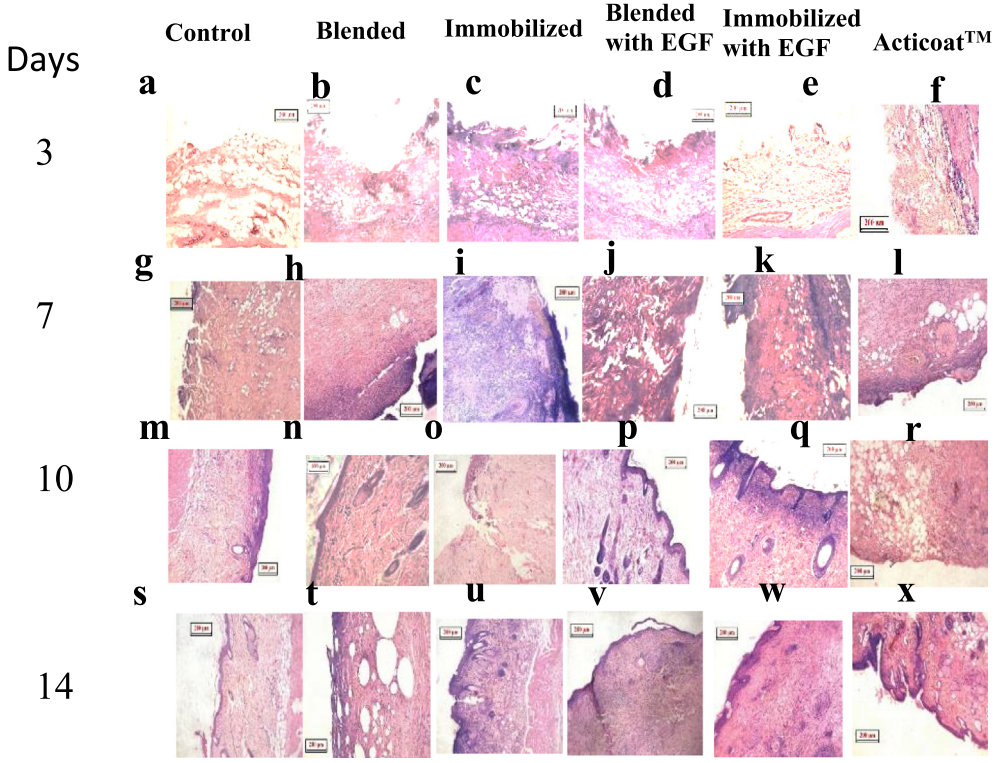

Fig. 8A. Represents H&E staining of nondiabetic control (a, g, m, n), blended (b, h, n, t), immobilized (c, i, o, u), blended with EGF (d, j, p, v), immobilized with EGF (e, k, q, w), Acticoat (f, l, r, x) after 3, 7, 14, 21 days post- wounding at 10× magnification. Scale bar 200 μm.

characteristically reduced in diabetic wounds with no specific organization (Fig. 10B(s)–(x)). It could be anticipated that apoptosis during the healing process might have caused impaired repair process as endothelial cells, fibroblasts and pericytes undergone premature death before they could carry out their normal healing functions [53]. However, in hyperglycemic wound, rEGF deprived PU/SF groups still exhibited alpha sma in well pattern within granulation tissue (Fig. 10B(v) and (w)) indicating absence of rEGF, lowered the rate of apoptosis. In the diabetic control wounds, staining of fibroblasts and macrophages adjacent to the wound was apparent. In contrast, smooth muscle actin expression was relatively profuse in Acticoat™ and rEGF incorporated PU/SF treated groups compared to other groups (Fig. 10A(x), (t), and (u)) of normal burn. Except control and blended PU/SF, binding of highly cationic smooth muscle actin to components of the ECM such as glycosaminoglycans may also prolong the local activity of the healing factors at the wound.

4. Discussion

SF immobilized IPDI based PU scaffold proved its surface potential as an efficient wound dressing patch. When PU/SF scaffold modified with rEGF, it exhibited twofold enhanced performance compared to bare one. Mulberry SF-based scaffolds though have been reported earlier to show promising outcome for ECM development but when mulberry SF protein dosage is preselected based on effective anti-bactericidal concentrations, incorporated with rEGF and combined with highly biocompatible, degradable, high swellable and tailorable IPDI based PU, it exploits the combinatorial potential of PU, SF. Moreover, rEGF incorporation and NIH3T3 cell seeding on PU/SF scaffold aid in comparative faster healing progression in hyperglycemic wound. Though SF is mainly comprised of hydrophobic amino acids (glycine and alanine) and serine, its structural orientation improves hydrophilicity which reduces contact angles of the PU/SF scaffold surface, facilitating higher affinity to cell proliferation. Growth factors like rEGF and fibroblast growth factor (FGF) are obvious to regulate different key factors of wound healing in all stages [54], therefore rEGF release assisted in healing progression. SF and rEGF release required no external drug or antimicrobial, anti-inflammatory agent or antioxidant molecules to restore the oxidative damage or elevated inflammatory mediators. Infection free dry wound bed is of paramount importance at exuding wound, blood platelet adhesion and thrombogenicity [55], appreciable fluid retention capacity, immuno-modulatory role towards inflated oxidative

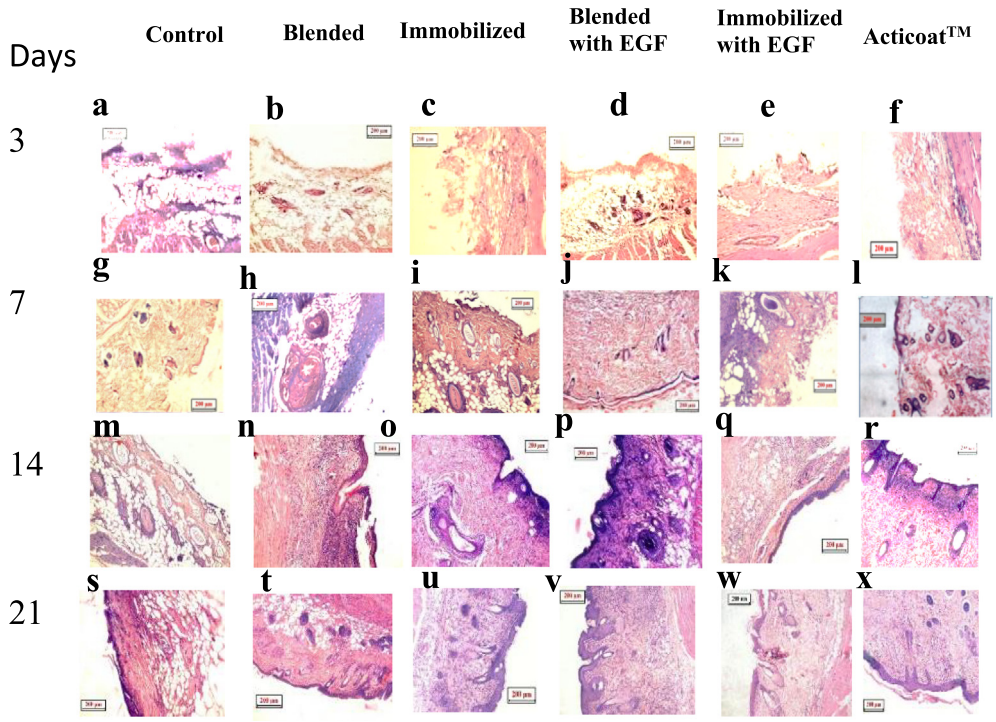

Fig. 8B. Represents H&E staining of diabetic control (a, g, m, n), blended (b, h, n, t), immobil ized (c, i, o, u), blended with EGF (d, j, p, v), immobilized with EGF (e, k, q, w), Acticoat (f, l, r, x), after 3, 7, 14, 21 days post- wounding at 10× magnification. Scale bar 200 μm.

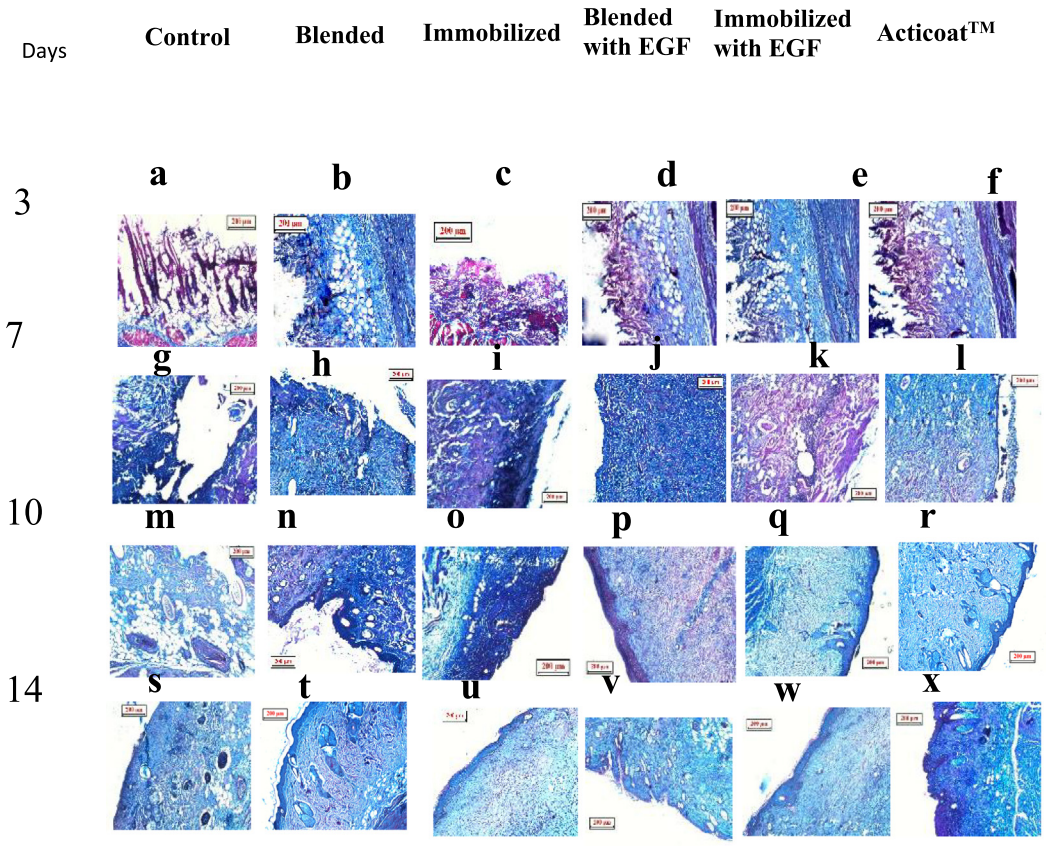

Fig. 9A. Represents Masson's trichome staining of nondiabetic control (a, g, m, n), blended (b, h, n, t), immobilized (c, i, o, u), blended with EGF (d, j, p, v), immobilized with EGF (e, k, q, w), Acticoat (f, l, r, x) in normal burn wound after 3, 7, 14, 21 days post-wounding at 10× magnification. Scale bar 200 μm.

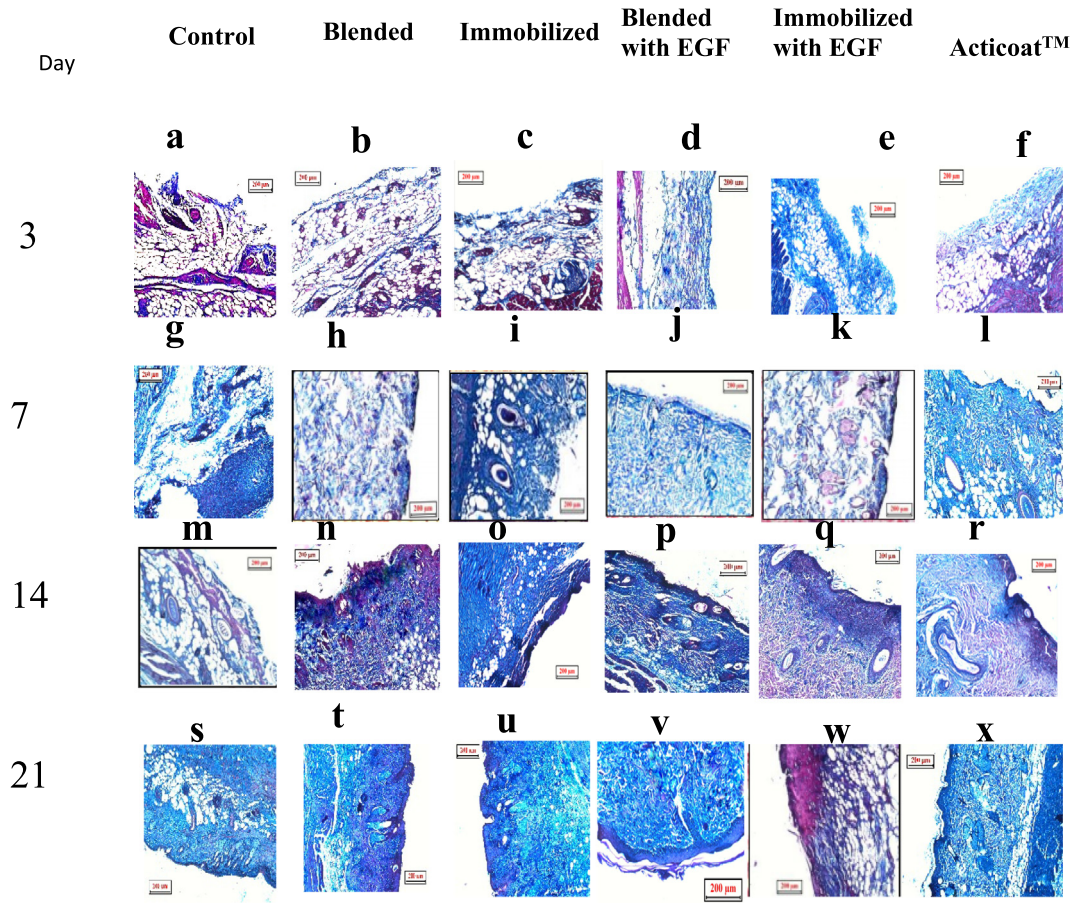

Fig. 9B. Represents Masson's trichome staining of control (a, g, m, n), blended (b, h, n, t), immobilized (c, i, o, u), blended with EGF (d, j, p, v), immobilized with EGF (e, k, q, w), Acticoat (f, l, r, x) in diabetic condition of burn wound after 3, 7, 14, 21 days post-wounding at 10× magnification. Scale bar 200 μm.

stress made PU/non-mulberry SF hybrid scaffolds superior over commercial Acticoat™. Another advantageous side includes that PU/SF topical treatment required to replace at 10–11 days whereas Acticoat™ required mandatory change after 3 days in wet condition as indicated in manufacturer's protocol.

Full thickness scarless ninety percent affected area of hyperglycemic wound was healed within 24 days and nondiabetic burn was healed by 16 days (Fig. 7(A) and (B)) with NIH3T3 cell seeded immobilized PU/SF matrix leaving no scar and regenerated skin had equally comparable mechanical strength (Fig. 3(a) and (b)) with that of unburnt skin indicating good quality regeneration of epidermis. Wound healing was achieved with very prospective feature of restoration of elevated serum and tissue inflammatory cytokine IL-6, IL-8 and IL-10 level showing cushioning effect against oxidative stress of third degree burn. A marked difference was observed in tissue IL-6, IL-8 and IL-10 quantity as interleukin values raised to the highest in control group followed by blended PU/SF groups, Acticoat™ and least for rEGF treated immobilized PU/SF scaffolds in descending order at 48 h of post non-diabetic burn. On the contrary, rEGF deprived immobilized PU/SF treated group provided closest interleukin values to that of sham (unburnt rat skin) at 48 h diabetic postburn complying with the efficiency of immobilized PU/SF scaffold and it corroborates that rEGF did not play significant role in pro-inflammatory cytokine restoration. At 2nd week of post burn, rEGF containing immobilized PU/SF treated group provided lesser values of serum IL-6, IL-8 and IL-10 level, compared to that of Acticoat™ treated group in non-diabetic burn suggesting its superiority in terms of tight regulation of inflammatory cytokines which might have caused due to potential shock absorbance from oxidative stress of third degree burn. The reactive oxygen and nitrogen species scavenging properties of PU/SF composites could have removed the reactive free radicals, which could be responsible for sudden elevation of IL-6, IL-8 and IL-10. Though detailed insight of free radical scavenging ability of mulberry SF is not available yet, however, it might be attributed by underlying antioxidant properties of SF that had contributed to inhibition of proinflammatory cytokines as they are usually triggered by reactive oxygen species. The anticipated antioxidant activity of SF could be due to prevalence of hydroxyl amino acids like serine and threonine imparting remarkable amount of hydroxyl groups of such amino acids that could chelate trace elements causing the radical scavenging. It is further supported SF acts as a powerful inhibitor against hydrogen peroxide damage in keratinocytes and fibroblasts as it suppressed proinflammatory cytokine (IL-6, IL-10) response. Active NIH3T3 (at 3rd day culture in scaffold) cells in diabetic wound had attenuated intervening effects on excess collagenization; which had reduced inflammatory molecules production [56].

Serum IL-6, IL-10 level in diabetic wound where cytokine restoration by both EGF loaded blended and immobilized PU/SF groups was lesser compared to EGF deprived blended and immobilized variety (Fig. 5(b) and (d)) and it was reverse for tissue IL-6 and IL-10 (Fig. 5(f) and (h)). MMPs have certain correlation with inflammatory cytokines [57]. Tissue, serum IL-10 and IL-6 showed positive correlation with MMP-9, that EGF loaded treatment groups expressed more MMP 9 and restored tissue IL-10 and IL-6 faster. However, statistically significant conflicting serum IL-6 kinetic profile with MMP 9 in diabetic group could be due to eval-

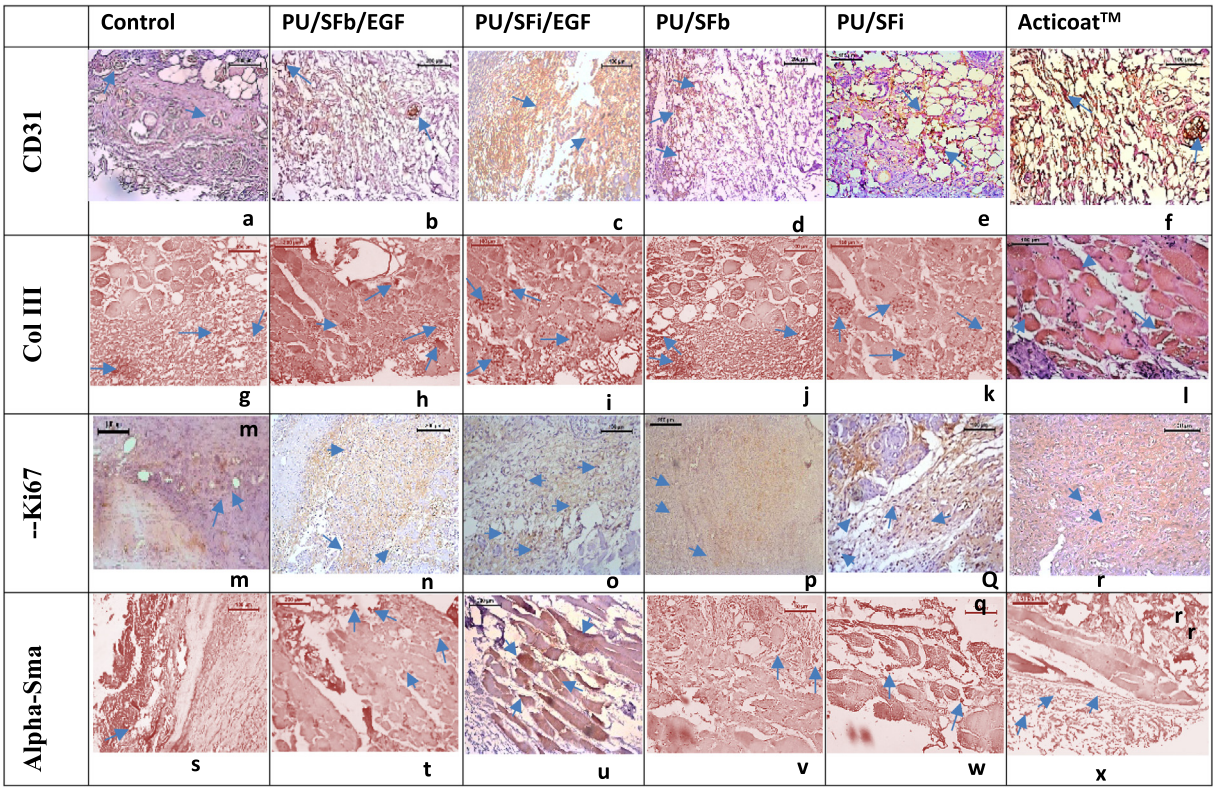

Fig. 10A. Representative IHC images of anti-CD31 stained histological sections on day 7; anti-Ki67 on day 7; anti-Col III on day 14 and anti-apha sma on 10 day after initial nondiabetic burn wound. Anti-CD31, anti-alpha sma images were taken at 20× (Scale bar 100 μm), and anti-Ki67 and anti-COL III images were taken at 10× (Scale bar 200 μm) magnification.

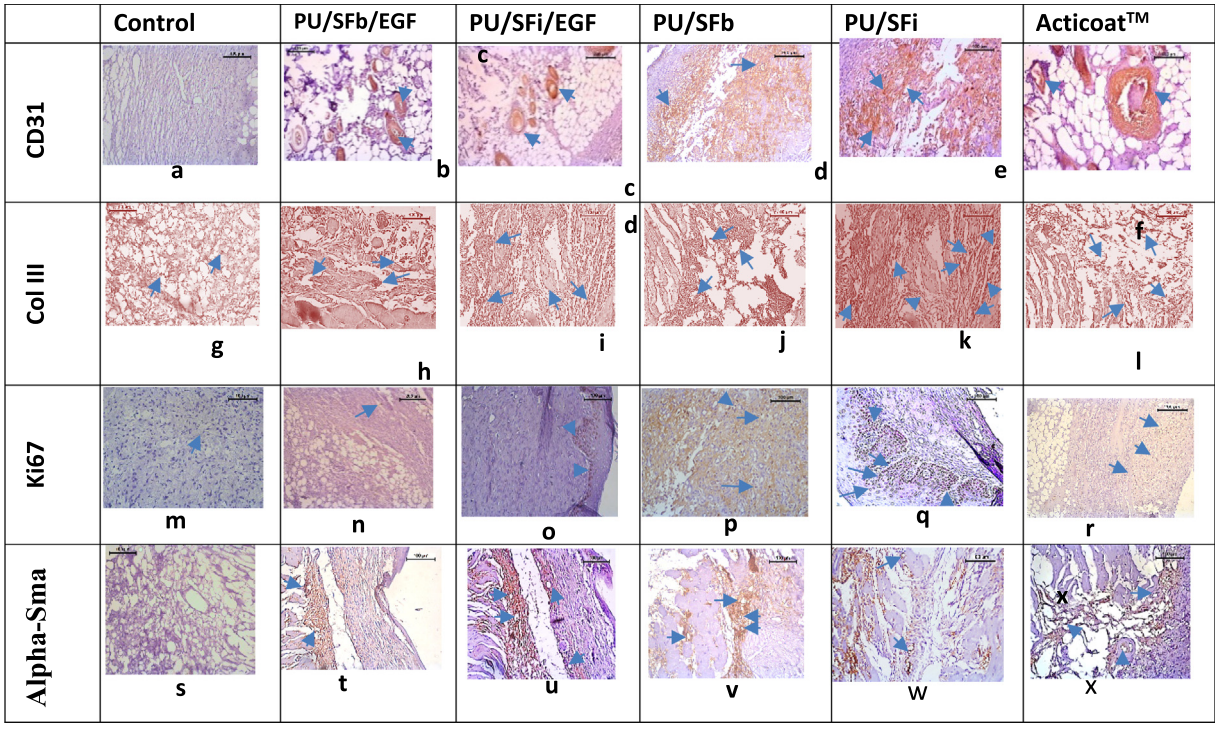

Fig. 10B. Representative IHC images of anti-CD31 stained histologic al sections on day 7; anti-Ki67 on day 7; anti-Col III on day 14 and anti-apha sma on 10 day after initial diabetic burn wound. Anti-CD31, anti-alpha sma images were taken at 20× (Scale bar 100 μm), and anti-Ki67 and anti-COL III images were taken at 10× (Scale bar 200 μm) magnification.

uation of MMP 9 was done from wound tissue homogenate. MMP 9 plays pivotal role in cell migration and invasion [58] and EGF administration has implication in MMP 9 activation through EGFR (Epidermal growth factor receptor) [59]. In earlier studies it was demonstrated EGF and TGF-β1 synergistically stimulate cell migration through increased MMP-9 function and increased extracellular signal-regulated kinase ERK1/2 activation. Extracellular signal-controlled kinase (ERK) signals demonstrate ERK1/2 activation is strongly induced by EGF [60]. Overall, it is evident that combined role of SF and EGF, mediated the alleviation of burn-induced oxidative damage by restoring the elevated pro-inflammatory cytokines (IL-6, IL-8, IL-10) secreted by leukocytes and macrophages through regulation of MMP 9. In epithelial cells, EGF is involved in tuning E-cadherin/β-actin complex as well [61]. Since it was reported E-cadherin protein expression reverses in presence of EGF stimulation and EGFR regulates E-cadherin expression and its complex formation [62], thus higher accumulation of gap junction establishing protein E-cadherin (Fig. 6(b)) by PU/SF blended (without rEGF) and immobilized (without rEGF) treatment groups could be justified.

Histological scoring results complied with the findings of pro-inflammatory cytokines response. Treatment groups with rEGF, scored less in diabetic wound closure and IL-6, IL-8 and IL-10 level restoration by rEGF incorporated groups was also lesser than rEGF deprived immobilized groups. In nondiabetic wound, at 10th day, immobilized PU/SF and rEGF loaded blended PU/SF scored (4.2) equally giving insight that synergistic effect of rEGF and SF release from PU/SF blended was equally competitive to higher release rate of SF alone from immobilized PU/SF scaffolds. Likewise, in diabetic wound, at 3rd day, blended PU/SF and rEGF loaded immobilized PU/SF scored equally (1.6). This could be substantiated that combined effect of SF and rEGF release from immobilized variety negated the effect of slower releasing effect of SF from blended one. Thus, it could be inferred that intervening effect of rEGF, released from rEGF loaded immobilized PU/SF suppressed the effect of higher SF release from the same scaffold. rEGF loaded immobilized PU/SF. Remodelling in maturation phase imparts functionality to healed tissue where isotropic alignment of collagen fibers yielded to functional tissue regeneration which was obtained in rEGF loaded NIH3T3 cell seeded immobilized PU/SF and NIH3T3 cell seeded immobilized PU/SF scaffolds for normal and diabetic wound respectively. In contrast, systemic orientation of collagen fibers allowed less-functional scar regeneration which is relevant to 21 days MT staining of Acticoat treated tissue [63]. Excess scar formation induces lack of skin functionality; causing inability to develop secondary features like skin appendages like hair, sebaceous glands and protruding nerve endings [24]where control (Fig. 8B(s)), blended, EGF loaded blended PU/SF (Fig. 8B(t) and (v)) and Acticoat (Fig. 8B(x)), showed the shortcoming in contrast to occurrence of essential skin appendages in HE and MT staining of NIH3T3 loaded immobilized PU/SF treated group reconfirmed superiority in diabetic wound at 21 days. Hence it may be presumed that **r**EGF administration did not much effect in diabetic healing, but cellular immobilized PU/SF group significantly contributed to both type healing progression as it attracted more NIH3T3 cells and this is justified because loaded fibroblasts are enriched source of cytokines and essential growth factors which together with substantial amount of released SF performed the best [27].

Immunohistochemical staining confirmed signature protein expression at different phases like onset of neovascularization and hemostatic activity were confirmed by expression of alpha smooth muscle actin at 10th day followed by angiogenesis observed by CD31 at 7th day, proliferative feature by accumulation of Ki67 at 7th day and maturation phase by COL III at 14th day. Morphometric studies of smooth muscle actin staining were predominantly extracellular, within the fibrin clot and in the ECM of dermis suggests that most of the smooth muscle actin present in the wound was released from de-granulating platelets and bound to ECM mainly. CD-31 stained endothelial cells, macrophage, platelets, reflected greater orientation of vascularity coming closer to normal subcutaneous vessel architecture, vascular architecture dictates nutritive blood flow in PU/SF blended and immobilized groups whereas chaotic vessel arrangement reflects the impaired blood flow in control. In epidermal layer at immediate vicinity to wound region, dense population of Ki 67 positive basal cells found in Acticoat™ and immobilized PU/SF as wave-like pattern in non-diabetic wound with advancing distance from wound edges. Ki67 positive fibroblasts decrease markedly with advancing distance from wound edge reflects fibroblast cells localized in dermis adjacent to burnt area could be responsible for granulation tissue development [27]. The tubular shapes, and number of Col III cells significantly increased relative in number in the treatment groups compared to control (Fig. 10A(t), (n), (w), and (x)). In hyperglycemic group, number of alpha sma positive cells were dramatically lower in all the groups except the rEGF loaded groups (Fig. 10B(t) and (u)). In all the phases, characteristic markers responded coherently by rEGF incorporated groups and rEGF deprived immobilized groups. Therefore, it is well interpreted that NIH3T3 seeded SF in the route of immobilization on PU with or without rEGF has reinforced its healing potential in an advancing approach both in diabetic and normal burn wound, thus it can be considered as full thickness dermal substitute for future applications in diabetic burn.

5. Conclusion

Controlling blood sugar levels, wound infection have significant impact on the healing process. Thus, consistent blood sugar level was maintained throughout the experiment to assert the efficiency of different treatment groups on hyperglycemic wound healing. The outcome of the study reflects, immobilized fabrication route has greater potential to release both SF and rEGF synergistically, thus successfully healed diabetic wound at 16 days avoiding microbial load at wound bed. Irrespective of the role of rEGF; immobilized PU/SF scaffold variety has shown greater healing prospect compared to blended variety in either type of wound. Since wound matrix degradation is overly high in diabetes, role of MMP9 in ECM degradation and correlation with E-cadherin expression for all the scaffold treatment has been corroborated in western blot and gelatin zymographic results. Immunomodulatory response of rEGF containing immobilized treatment groups were nearly restored back to that of unburnt skin. Due to anti-inflammatory scaffolds can find application as drug carrier in disease model studies. While fabricating, if scaffolds are optimized with a different pore size, it can attract a multiple cell lineage. Such investigation with PU/SF composite scaffold would be useful for other tissue engineering applications.

Declaration of Competing Interest

Authors declare there is no conflict of interest.

Acknowledgement

Sohini Sen is grateful to Council of Scientific and Industrial Research for providing senior research fellowship (File no. 09/096 (786)/2013-EMR-I). We sincerely acknowledge the funding provided by TEQUIP-Phase II, Jadavpur University. The service at Central Instrument Service of AFM facility at Indian Association for the

Cultivation of Science and the Instrument Service of SEM facility at Jadavpur University is acknowledged.

Appendix A. Supplementary material

Supplementary data to this article can be found online at https://doi.org/10.1016/j.ijbiomac.2019.09.219.

References

[1] National Diabetes Information Clearinghouse, National Diabetes Statistics fact sheet <http://diabetes.niddk.nih.gov/dm/pubs/statistics/index.htm> (accessed April 2019).
[2] S. Wild, G. Roglic, A. Green, R. Sicree, H. King, Diabetes Care 27 (2004) 1047.
[3] World Health Organization, WHO Library Cataloguing-in-Publication Data - Global Report on Diabetes, World Health Organization, Geneva, 2016.
[4] C. Mock, M. Peck, M. Peden, E. Krug, A WHO Plan for Burn Prevention and Care, World Health Organization, Geneva, 2008.
[5] American Burn Association, Burn Incidence and Treatment in the United States: 2013 Fact Sheet, American Burn Association, Chicago, 2013.
[6] C. Smolle, J. Cambiaso-Daniel, A.A. Forbes, P. Wurzer, G. Hundeshagen, L.K. Branski, F. Huss, L.P. Kamolz, Burns 43 (2017) 249.
[7] C. Alemdaroglu, Z. Degim, N. Celebi, F. Zor, S. Ozturk, D. Erdogan, Burns 32 (2006) 319.
[8] K. Hori, C. Sotozono, J. Hamuro, K. Yamasaki, Y. Kimura, M. Ozeki, Y. Tabata, S. Kinoshita, J. Control. Rel. 118 (2007) 169.
[9] H.J. Yoo, H.D. Kim, J. Appl. Polym. Sci. 107 (2008) 331.
[10] P. Chiarini, S. Petrini, I.D. Bozzini, Pra and U, Armato, *Biomaterials* 24 (2003) 789.
[11] D. Prà, P. Petrini, A. Charini, S. Bozzini, S. Farè, U. Armato, Tiss. Eng. 9 (2003) 1113.
[12] H.J. Yoo, H.D. Kim, J. Biomed. Mater. Res. Part B: Appl. Biomater. 85 (2008) 326.
[13] M. Rottmar, M. Richter, X. Mäder, K. Grieder, K. Nuss, A. Karol, B. von Rechenberg, E. Zimmermann, S. Buser, A. Dobmann, J. Blume, A. Bruinink, Sci. Technol. Adv. Mater. 16 (2015) 034606.
[14] Patra, S. Talukdar, T. Novoyatleva, S.R. Velagala, C. Mühlfeld, B. Kundu, S.C. Kundu, F.B. Engel, Biomaterials 33 (2012) 2673.
[15] Kaur, R. Rajkhowa, T. Afrin, T. Tsuzuki, X. Wang, Biopolymers 101 (2014) 237.
[16] D. Chouhan, B. Chakraborty, S.K. Nandi, B.B. Mandal, Acta Biomaterial. 48 (2017) 157.
[17] J. Hur, H.T. Yang, W. Chun, J.H. Kim, S.H. Shin, H.J. Kang, H.S. Kim, Ann. Lab. Med. 35 (2015) 105.
[18] Friji Meethale Thiruvoth, Devi Prasad Mohapatra, Dinesh Kumar, Sivakumar Ravi Kumar Chittoria, Vijayaraghavan Nandhagopal, Current concepts in the physiology of adult wound healing, Plast. Aesthet. Res. 2 (2015) 250–256.
[19] G. Zhao, P.C. Hochwalt, M.L. Usui, R.A. Underwood, P.K. Singh, G.A. James, P.S. Stewart, P. Fleckman, J.E. Olerud, Wound Repair Regener. 18 (2010) 467.
[20] Kuwahara, M. Hatoko, H. Tada, A. Tanaka, J. Cutan. Pathol. 28 (2001) 191.
[21] B.B. Mandal, S.C. Kundu, Biomaterials 30 (2009) 5019.
[22] S. Bhowmick, V. Koul, Mater. Sci. Eng.: C 59 (2016) 109.
[23] A. Haldar, S. Sen, D. Banerjee, N.K. Jana, P. Basak, Synthesis and characterization of biodegradable Polyether urethane for the purpose of controlled release of antibiotics, in: A. Padinjakkara, A. Thankappan, F.G. Souza, S. Thomas (Eds.), *Biopolymers and Biomaterials*, E-Publishing Inc., New Jersey, 2018, pp. 253–266.
[24] Y. Zhu, C. Gao, X. Liu, J. Shen, Biomacromolecules 3 (2002) 1312.
[25] N. Arora, A. Ali, S. Sen, N.K. Jana, P. Basak, Compos. Interf. 21 (2013) 51.
[26] P. Basak, S. Sen, Advanced Materials Research 584 (2012) 474.
[27] Y. Zhu, C. Gao, T. He, J. Shen, Biomaterials 25 (2004) 423.
[28] G. Totea, D. Ionita, I. Demetrescu, M. Magdalena Mitache, Central Euro. J. Chem. 12 (2014) 796.
[29] D. Chouhan, G. Janani, B. Chakraborty, S.K. Nandi, B.B. Mandal, J. Tiss. Eng. Regener. Med. 12 (2018) 1559.
[30] M. Panchatcharam, S. Miriyala, V.S. Gayathri, L. Suguna, Molecular and Cellular Biochemistry 290 (2006) 87.
[31] L.A. Elson, W.T.J. Morgan, Biochem J. 27 (1933) 1824.
[32] J.F. Woessner Jr, Arch. Biochem. Biophys. 93 (1961) 440.
[33] R.E. Neuman, A.A. Logan, J. Biol. Chem. 186 (1950) 549.
[34] A. Gupta, N.K. Upadhyay, R.C. Sawhney, Ratan Kumar, Wound *Repair and*, Regeneration. 16 (2008) 784.
[35] P.G. Bowler, B.I. Duerden, D.G. Armstrong, Clin. Microbiol. Rev. 14 (2001) 244.
[36] J.J. Akershoek, M. Vlig, W. Talhout, B.K.H.L. Boekema, C.D. Richters, R.H.J. Beelen, K.M. Brouwer, E. Middelkoop, M.M.W. Ulrich, Cell Tiss. Res. 364 (2016) 83.
[37] Q.L. Loh, C. Choong, Tiss. Eng. Part B: Rev. 19 (2013) 485.
[38] J. Rnjak-Kovacina, A.S. Weiss, Tissue Engineering Part B: Reviews 17 (2011) 365.
[39] T. Muthukumar, K. Anbarasu, D. Prakash, T.P. Sastry, Coll. Surf. B: Biointerf. 121 (2014) 178.
[40] E. Hablot, D. Zheng, M. Bouquey, L. Avérous, Macromol. Mater. Eng. 293 (2008) 922.
[41] P. Uttayarat, S. Jetawattana, P. Suwanmala, J. Eamsiri, T. Tangthong, S. Pongpat, Fibers Polym. 13 (2012) 999.
[42] K. Bankoti, A.P. Rameshbabu, S. Datta, P.P. Maity, P. Goswami, P. Datta, S.K. Ghosh, A. Mitra, S. Dhara, Mater. Sci. Eng.: C 81 (2017) 133.
[43] H. Sobel, H.A. Zutrauen, J. Marmorston, Arch. Biochem. Biophys. 46 (1953) 221.
[44] D. Agay, M. Andriollo-Sanchez, R. Claeyssen, L. Touvard, J. Denis, A.M. Roussel, Y. Chancerelle, Euro. Cytok. Netw. 19 (2008) 1.
[45] Q. Fang, S. Guo, H. Zhou, R. Han, P. Wu, C. Han, Scient. Rep. 7 (2017) 1.
[46] G. Kaur, S. Carnelio, N. Rao, L. Rao, Ind. J. Dental Res. 20 (2009) 71.
[47] H. Cho, S. Balaji, N.L. Hone, C.M. Moles, A.Q. Sheikh, T.M. Crombleholme, S.G. Keswani, D.A. Narmoneva, Wound Rep. Regen. 24 (2016) 829.
[48] A. Moirangthem, B. Bondhopadhyay, M. Mukherjee, A. Bandyopadhyay, N. Mukherjee, K. Konar, S. Bhattacharya, A. Basu, Scient. Rep. 6 (2016) 1.
[49] S.M. Kouhbananinejad, A. Derakhshani, R. Vahidi, S. Dabiri, A. Fatemi, F. Armin, A. Farsinejad, Biomaterials Science (2019) (Advance Article).
[50] P. Erba, R. Ogawa, M. Ackermann, A. Adini, L. Miele, P. Dastouri, D. Helm, S. Mentzer, R. D'Amato, G. Murphy, M. Konerding, D. Orgill, Ann. Surg. 253 (2011) 402.
[51] M. Vinish, W. Cui, E. Stafford, L. Bae, H. Hawkins, R. Cox, T. Toliver-Kinsky, Wound Rep. Regen. 24 (2016) 6.
[52] J.J. Tomasek, J. McRae, G.K. Owens, C.J. Haaksma, Am. J. Pathol. 166 (2005) 1343.
[53] I.A. Darby, T. Bisucci, T.D. Hewitson, D.G. MacLellan, Int. J. Biochem. Cell Biol. 29 (1997) 191.
[54] G.H. Altman, F. Diaz, C. Jakuba, T. Calabro, R.L. Horan, J. Chen, H. Lu, J. Richmond, D.L. Kaplan, Biomaterials 24 (2003) 401.
[55] B. Kundu, C.J. Schlimp, S. Nürnberger, H. Redl, S.C. Kundu, Scient. Rep. 4 (2014) 1.
[56] A.L. Laiva, F.J. O'Brien, M.B. Koegh, J. Tiss. Eng. Regen. Med. 12 (2018) e296.
[57] W.T. L, H. S, L.W. Chow, Biomed. Pharmacother. 61 (2007) 548–552.
[58] S.S. Lin, K.-C. Lai, S.-C. Hsu, J.-S. Yang, C.-Lin Kuo, J.-Pin Lin, Yi-S. Ma, Chih-Chung Wu, J.-G. Chung, Cancer Lett. 285 (2009) 127–133.
[59] S.B. Kondapaka, R. Kridman, K.B. Reddy, Int. J. Cancer 70 (1997) 722–726.
[60] P. Adiseshaiah, M. Vaz, N. Machireddy, D.V. Kalvakolanu, S.P. Reddy, J Cell Physiol. 2 (2008) 405.
[61] M. Kuwahara, M. Hatoko, H. Tada, A. Tanaka, J. Cut. Pathol. 28 (2001) 191.
[62] O. Alper, M.L.D. Santis, K. Stromberg, N.F. Hacker, Y.S. Cho-Chung, D.S. Salomon, Int. J. Can. 88 (2000) 566.
[63] J. Godwin, D. Kuraitis, N. Rosenthal, Int. J. Biochem. Cell Biol. 56 (2014) 47.
[64] P. Maurye, A. Basu, S. Sen, J. Biswas, T. Bandyopadhyay, M. Naskar, User-friendly tool kits for protein gel electrophoresis techniques: A training program for high school students, Bichem. Mol. Biol. Edu. 47 (5) (2018) 566–577, https://doi.org/10.1002/bmb.21172.